UNIVERSITY OF TARTU
Faculty of Science and Technology
Institute of Technology

Nargiz Kazimova

Shungite as a Catalyst Support for Highly Active Bifunctional Oxygen Electrocatalyst

Bachelor's Thesis (12 ECTS)

Curriculum Science and Technology

Supervisors:
Senior Researcher, Ph.D. Nadezda Kongi
Associate professor, Ph.D. Kaido Tammeveski

Tartu 2020

Shungite as a Catalyst Support for Highly Active Bifunctional Oxygen Electrocatalyst

Abstract:

Metal-air batteries (MABs) and regenerative fuel cells (RFCs) are based on oxygen evolution reaction (OER) and oxygen reduction reaction (ORR). Creating efficient bifunctional oxygen electrocatalysts to promote both OER and ORR simultaneously is highly desirable but full of great challenges. The major limitation is that active ORR catalysts are often not efficient for OER, and vice versa. Therefore, the development of novel bifunctional oxygen electrocatalyst should ensure the exhibition of high activity for both reactions. In this work, electrochemically active and stable bifunctional catalyst materials were prepared from naturally occurred shungite-derived carbon material doped with nitrogen, iron, and cobalt. Prior doping, the purification of raw shungite powder was optimized and the surface morphology, structure and porosity of all samples were extensively investigated by SEM, HRTEM, XRD, Raman spectroscopy, and the BET method. Bifunctional electrocatalytic activity and stability of shungite-based materials were examined toward ORR and OER in 0.1 M KOH solution by the rotation disk electrode (RDE) method. Shungite-based catalyst doped with iron and cobalt had much lower OER overpotentials compared to commercial RuO_2 benchmark and the overall oxygen electroactivity parameter (ΔE) was close to that obtained for noble metal-based commercial electrocatalysts (Pt/C + RuO_2). Electrochemical stability of bimetallic shungite-based catalysts examined by the chronoamperometry technique was superior to that obtained with commercial electrocatalysts.

Keywords:

Shungite, Bifunctional electrocatalyst, Nitrogen doping, Oxygen reduction reaction, Oxygen evolution reaction

CERCS: P401 Electrochemistry

Šungiidil põhinevad aktiivsed bifunktsionaalsed hapniku elektrokatalüsaatorid

Lühikokkuvõte:

Metall-õhk akudes (MAB) ja regeneratiivsetes kütuseelementides (RFC) on olulised hapniku eraldumisreaktsioon (OER) ja hapniku redutseerumisreaktsioon (ORR). Tõhusate bifunktsionaalsete ORR/OER katalüsaatorite loomine on suur väljakutse. Peamine piirang on see, et aktiivsed ORR-katalüsaatorid ei ole OER-i jaoks sageli efektiivsed ja vastupidi. Seetõttu peaks uudsete bifunktsionaalsete hapniku elektrokatalüsaatorite väljatöötamine tagama kõrge aktiivsuse mõlemale reaktsioonile. Selles bakalaureusetöös valmistati elektrokeemiliselt aktiivsed ja stabiilsed katalüsaatorid kasutades looduslikult esinevast šungiidist saadud süsinikmaterjali dopeerimist lämmastiku, raua ja koobaltiga. Eelnevalt optimeeriti šungiidipulbri puhastamisprotseduuri ning seejärel uuriti materjalide pinna morfoloogiat, struktuuri ja poorsust kasutades SEM, HRTEM, XRD, Ramani spektroskoopia ja BET meetodit. Šungiidipõhiste materjalide bifunktsionaalset elektrokatalüütilist aktiivsust ja stabiilsust uuriti pöörleva ketaselektroodi (RDE) meetodil ORR ja OER suhtes 0,1 M KOH lahuses. Raua ja koobaltiga dopeeritud šungiidipõhistel katalüsaatoritel oli OER-i ülepinge palju madalam kui kommertsiaalsel RuO_2 katalüsaatoril ja hapniku elektroaktiivsuse parameeter (ΔE) oli lähedane väärismetallidel põhinevate kommertsiaalsete elektrokatalüsaatorite (Pt/C + RuO_2) omale. Kronoamperomeetria meetodil uuritud bimetalsete šungiidil põhinevate katalüsaatorite elektrokeemiline stabiilsus oli parem võrreldes kommertsiaalsete elektrokatalüsaatorite stabiilsusega.

Võtmesõnad:

Šungiit, Bifunktsionaalne elektrokatalüsaator, Lämmastikuga dopeerimine, Hapniku redutseerumise reaktsioon, Hapniku eraldumise reaktsioon

CERCS: P401 Elektrokeemia

TABLE OF CONTENTS

TERMS, ABBREVIATIONS AND NOTATIONS

BET – Brunauer-Emmett-Teller

$CoCl_2$ – cobalt (II) chloride

CV – cyclic voltammetry

DCDA – dicyandiamide

E – electrode potential

$E_{1/2}$ – half-wave potential

EDS – energy dispersive X-ray spectroscopy

E_{onset} – onset potential

FC – fuel cell

$Fe(OAc)_2$ – iron (II) acetate

GC – glassy carbon

HER – hydrogen evolution reaction

j – current density

K-L – Koutecký–Levich

MABs – metal-air batteries

MEL – melamine

OER – oxygen evolution reaction

ORR – oxygen reduction reaction

PVP – polyvinylpyrrolidone

RHE – reversible hydrogen electrode

η – overpotential

SEM – scanning electron microscopy

SHE – standard hydrogen electrode

TEM – transmission electron microscopy

XRD – X-ray diffraction

INTRODUCTION

New technologies for sustainable energy production, storage and conversion have gained considerable interest in academia and industry, due to the accelerated exhaustion of fossil fuels along with environmental pollution. Rechargeable metal-air batteries (MABs), fuel cells (FCs), and water splitting are the next-generation clean power devices. The oxygen reduction reaction (ORR) and oxygen evolution reaction (ORR), which are main reactions in these electrochemical energy devices, require a catalyst to be functional in a wide range of applications. Nowadays, the precious-metal-based catalysts (Pt/IrO_2, RuO_2) show the best electrocatalytic performance toward ORR and OER. Major drawbacks of current *state-of-the-art* noble metal catalysts are their scarcity, high price, and poor electrochemical stability [1]. Moreover, current precious-metal-based electrocatalysts are non-bifunctional toward ORR/OER and do not meet practical requirements for energy technology applications. Consequently, the design of an efficient and inexpensive alternative, which will be able to catalyze both reactions simultaneously, is highly crucial for large-scale applications. One of the most promising alternatives, which demonstrate excellent electrocatalytic behavior is high-surface-area carbon-based materials that are co-doped with transition metals and heteroatoms. Extensive research has been conducted on exploring different carbon sources and metal and nitrogen precursors to create the most efficient and practical electrocatalyst with high activity for both ORR and OER. Graphene has been mainly studied as a catalyst support, but also it plays an important role in the development of non-precious metal catalysts, particularly in pyrolyzed transition metal–nitrogen–carbon composites.

Shungite is a natural carbon-rich mineraloid deposited mainly in the Karelia region (Russia) and its total reserve is estimated more than 250 gigatons [2]. The graphene-based basic structure of shungite provides a good reason to consider this material as a promising alternative to synthetic graphene in various applications. Moreover, the production of synthetic graphene oxide flakes is much less environmentally friendly than that compared to shungite-derived graphene oxide.

Herein, for the first time, shungite-derived carbon material was doped with nitrogen, cobalt, and iron. Surface morphology, porosity and structure of the prepared catalysts was studied by SEM, HR-TEM, BET, XRD, and Raman spectroscopy. Shungite-based materials were tested in 0.1 M KOH solution toward oxygen reduction reaction and oxygen evolution reaction. Chronoamperometry was used to evaluate the stability of the prepared electrocatalysts.

1 LITERATURE REVIEW

1.1 Oxygen electrocatalysis

Growth of global energy demand and carbon-neutral energy economy are among the matter of interests in the 21st century. Nowadays, most of the energy originates from unsustainable fossil fuels, meaning finite resources [3]. This drives to the development of new, eco-friendly, and cost-effective technologies that produce renewable and sustainable energy. Fuel cells (FCs), water splitting, and metal-air batteries (MABs) are the most efficient and simple devices of different conversion energy systems running through electrochemical reactions.

Electrochemical reduction and evolution of oxygen (O_2) are the key reactions in renewable energy technologies. During the oxygen reduction reaction (ORR) oxygen molecule combines with electrons to form a product, whereas during oxygen evolution reaction (OER) oxygen is produced by consuming electrons from a reactant (Scheme 1).

Both OER and ORR are vital in rechargeable metal-air batteries, where during the discharge process, oxidation reactions occur on the metal anode with metal dissolved in the electrolyte and ORR is induced on the air cathode [4,5].

ORR is the main reaction in the fuel cell cathode and is a major limiting factor of fuel cell performance [6]. Moreover, the OER is an anodic reaction, which, in conjunction with the cathodic hydrogen evolution reaction (HER), is crucial for the electrochemical water splitting [7].

The ORR and OER have sluggish kinetics, thus requiring an efficient electrocatalyst to be practical in numerous applications. To date, noble-metal-based catalysts are the most active for both ORR and OER [8–10]. Platinum-based catalysts show the best ORR activity, while being inefficient toward OER, whereas, Ru/Ir-based catalysts are best for OER [11]. Platinum (Pt) is not suitable metal for OER due to the oxidation of Pt surface at high positive potentials. Apart from high electrochemical performance, noble metal-based catalysts have certain disadvantages such as scarcity, high cost, poor electrochemical stability, and low selectivity [12]. Therefore, the design of alternative stable, and highly efficient bifunctional electrocatalysts, eligible of catalyzing the ORR and OER simultaneously, is crucial for wide-scale applications. The design of advanced bifunctional oxygen electrocatalysts is only possible if the nature of the electrochemical reaction active sites is fully understood [11].

By varying different physicochemical parameters during the synthesis of catalyst materials such as valence state, phase composition, morphology, surface defects, surface area, conductivity, etc., it is possible to increase the density of the electrocatalytically active sites and to tune the intrinsic electrocatalytic activity [11,13]. In the following paragraphs, the main up-to-date progress in the studies of ORR/OER electrocatalysis will be reviewed.

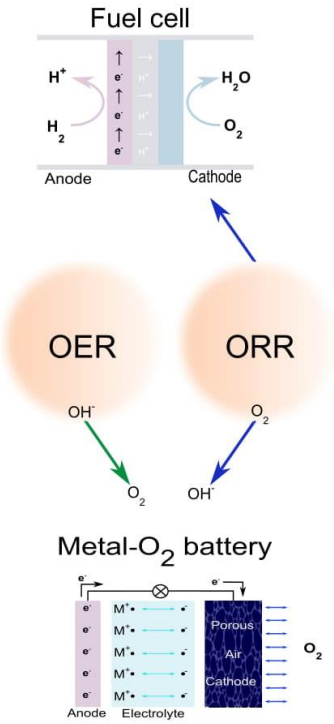

	ORR	OER
Acid media:	$O_2+4H^++4e^-\rightarrow 2H_2O$	$2H_2O\rightarrow O_2+4e^-+4H^+$
Alkaline media:	$O_2+2H_2O+4e^-\rightarrow 4OH^-$	$4OH^-\rightarrow O_2+4e^-+2H_2O$

Scheme 1. Schematic representation of OER and ORR reactions.

1.1.1 Oxygen reduction reaction

Oxygen is the most abundant element on the Earth and the reduction of O_2 is important not only in crucial life processes, such as biological respiration but also in energy conversion devices, such as fuel cells [14]. In aqueous solutions, the ORR can proceed via two different reaction pathways where the four-electron ($4e^-$) reduction occurs from oxygen to water (H_2O), and two-electron ($2e^-$) reduction from O_2 to hydrogen peroxide (H_2O_2) [15]. Typically, the $4e^-$ pathway prevails on noble metals, and the $2e^-$ pathway mainly occurs on carbonaceous materials [5,12]. In fuel cells, the ORR occurs at the cathode including following steps: (1) the diffusion and adsorption of O_2 molecules at the electrocatalyst surface, (2) e^-

are transported from electrode to adsorbed oxygen molecules, (3) weakening and breaking of O = O bonds, and (4) removing the produced OH^- ions into the electrolyte solution [10]. Depending on electrode material, the ORR proceeds through either a direct four-electron pathway or via indirect 2-step $2e^-$ pathway with intermediate formation of hydrogen peroxide, which reduces further to water. For a direct four-electron pathway, the reactions in acid and alkaline electrolytes are shown in Scheme 1. For indirect 2-step $2e^-$ pathway in alkaline solution after the formation of hydrogen peroxide (Eq. 1), 2-electron reduction of H_2O_2 (Eq. 2) or chemical disproportionation of peroxide occurs (Eq. 3) [10]:

$$O_2 + H_2O + 2e^- \rightarrow HO_2^- (-0.076 \text{ V vs. SHE}) \quad (1)$$

$$HO_2^- + H_2O + 2e^- \rightarrow 3OH^- (0.878 \text{ V vs. SHE}) \quad (2)$$

$$2HO_2^- \rightarrow 2OH^- + O_2 \quad (3)$$

In acidic media, indirect 2-step $2e^-$ pathway includes the following steps (Eqs. 4a, 4b) [10]:

$$O_2 + 2H^+ + 2e^- \rightarrow 2H_2O_2 (0.695 \text{ V vs SHE}) \quad (4a)$$

$$H_2O_2 + 2H^+ + 2e^- \rightarrow 2H_2O (1.776 \text{ V vs SHE}), \quad (4b)$$

where SHE stands for standard hydrogen electrode.

Since the O=O bond is exceptionally strong (bond energy of 498 kJ mol^{-1}), it is necessary to use electrocatalysts to lower the energy barrier and break the bond [16]. Currently, carbon-supported Pt has the highest ORR electrocatalytic activity, however, it has many drawbacks limiting it's wide application [17]:

(1) Pt is a finite resource and thus expensive;
(2) ORR on Pt proceeds partly by 2-step $2e^-$ pathway and intermediate hydrogen peroxide effects negatively on the cathode and membrane stability;
(3) Pt catalysts are highly sensitive to impurities in the FC feed system. Pt surface adsorbs easily NO_x and SO_x species present in FC air stream and this leads to decrease of the FC performance [18];
(4) In case if organic compounds are used as a fuel (for example, indirect methanol fuel cells (DMFC)), Pt cathode catalyst can easily be poisoned [19,20];

Significant effort is being made to develop Pt-free electrocatalysts for ORR, that would be efficient to catalyze oxygen by direct four-electron reduction without intermediate H_2O_2 production with low overpotential, be highly tolerant to contaminants and degradation [17].

Up to date, the most promising alternatives are metal-nitrogen-carbon (M-N-C, where M = Fe, Co, Ni, Mn, etc.) materials, where abundant metal and nitrogen are incorporated into nanocarbon [21–26]. In general, to prepare such M-N-C catalysts carbon, nitrogen and metal precursors are treated at high temperatures to yield conductive material with M-N_x sites, which are active toward ORR [27]. Pyrolyzed M-N-C catalysts obtained by heat-treatment in an inert gas atmosphere showed promising electrocatalytic activity and stability [27–29]. For further ORR activity and stability enhancement of pyrolyzed catalysts, modification of various factors such as nitrogen source and content, transition metal type and loading, heat treatment temperature and duration and variation of carbon supports are being conducted [28,30].

1.1.2 Oxygen evolution reaction

The oxygen evolution reaction (OER) is the process of generating O_2 usually from H_2O through an electrochemical reaction at the anode [31]. OER is the main reaction responsible for converting renewable electricity into storable fuels, however, due to the complicated multielectron transfer process it is kinetically sluggish [32]. The general OER mechanism over metal oxides in alkaline solutions is as follows [31]:

On the anode:

$$4OH^- \rightarrow 2O_2 + 2H_2O\ (l) + 4e^- \quad (5)$$

Following two intermediate processes:

$$OH^- + * \rightarrow OH_{ads} + e^- \quad (6)$$

$$OH_{ads} + OH^- \rightarrow O_{ads} + H_2O + e^- \quad (7)$$

where * designates the active sites of the catalyst surface and “ads” stands for the adsorption on the catalyst surface. The generation of O_2 is possible *via* two pathways. First is through the direct combination of two O_{ads} intermediates to form O_2 (g):

$$2O_{ads} \rightarrow O_2 \quad (8)$$

Another pathway involves the formation of the OOH_{ads} intermediate first by the interaction of O_{ads} with OH^-, with subsequent combination with OH^- and decomposed to O_2 gas. Here, the thermodynamic barrier of reaction (8) is always larger than those of reactions (9) and (10) [31]:

$$O_{ads} + OH^- \rightarrow OOH_{ads} + e^- \quad (9)$$

$$OOH_{ads} + OH^- \rightarrow O_2 + H_2O + e^- \quad (10)$$

Even though there are some differences in the reaction routes, it is widely accepted that the active sites for OER are the surface metal cations (M). Also, the metal-oxygen bond in the intermediates (M–OH, M–O and M–OOH) plays a crucial role in the electrocatalytic activity [32]. Strong metal-oxygen bond hinders the product desorption from the anode and weaker metal-oxygen bond prevents the binding of the intermediate on the surface of the anode [32]:

Platinum is not suitable for catalyzing OER, because, at the high positive potentials required for OER, the surface of Pt undergoes oxidation. Generally, iridium (Ir) and ruthenium (Ru) based catalysts possess very prominent performance [9,33–36]. However, similarly to platinum in ORR, these noble metals have their disadvantages to be widely implemented in practical applications.

The rapid increase in the amount of research on alternative and affordable catalyst with long-term stability and high activity have been established [37–40]. Transition metal phosphides [41], oxyhydrates [42], oxides [42–44], nitrides [45–48], perovskites [49,50], sulfides [51] were proposed as alternative OER catalysts. Fortunately, some of the non-noble metal-based electrocatalysts are capable to catalyze OER by outperforming noble-metal-based electrocatalysts in alkaline environment [44,52]. As an example, nickel, cobalt, and copper oxides show excellent catalytic performance toward OER [44]. Exhibiting promising OER electrocatalytic behavior, however, most of the materials are not capable to catalyze both OER and ORR simultaneously.

1.2 Bifunctional ORR/OER catalysis

1.2.1 Transition metal-based catalysts

Up to date, the most popular materials that have been explored as bifunctional oxygen electrocatalysts are metal oxides, hydroxides and sulfides, nanostructured carbon materials and different composite materials [4]. Due to their intrinsic activity and relatively high stability in oxidative electrochemical environments, transition metal oxides including Fe, Co, Ni, and Mn, have gained great attention as potential bifunctional ORR/OER catalysts [53]. The crystalline structure and chemical composition of such materials have great influence on the electrocatalytic performances [4]. For example, Jaramillo et al. demonstrated excellent bifunctional activity of Mn(III) oxide (Mn_3O_4), their observations confirmed that a disordered $Mn_3^{II,III,III}O_4$ phase contributes to the ORR, while a mixed $Mn^{III,IV}$ oxide is related to the OER performance [54]. Variations in morphology within the same phase also possess different

activity. For example, a mesoporous Co_3O_4 nanowire array showed highly efficient bifunctional ORR/OER electrocatalytic behavior compared to other morphologies [55]. Co_3O_4 nanowire arrays grown on Cu foil, exhibited higher OER and ORR activity (10 mA cm^{-2} at 1.52 V and half-wave potential of 0.78 V vs. RHE) in 0.1 M KOH solution and better stability in comparison to commercial IrO_2/C [55]. Atomic-level surface structure design can be used to fine-tune the exposure of active sites responsible for the electrocatalytic activity. Creating active facets with desirable atomic arrangement and coordination is the most efficient route in catalyst design [4]. Facet-dependent electrocatalytic performance of well-defined Co_3O_4 nanoparticles was investigated by Liu et al. who found that Co_3O_4 (111) has a lower activation barrier of O_2 desorption than Co_3O_4 (001) sites [56].

Various surface doping and metal-mixing can affect the electronic and/or surface structures of the catalyst materials toward better electrocatalytic activity. Therefore, spinel and perovskite structures with multi-metal components are widely used for ORR and OER electrocatalysis [4]. For example, highly active cubic $Co_xMn_{3-x}O_4$ materials were prepared and assembled in Zn-air batteries with a high energy density of about 650 W h kg^{-1} at 10 mA cm^{-2} normalized to consumed Zn anode [57]. Similarly, other spinel oxides, such as $NiCo_2O_4$ and $LiCoO_2$ have also shown excellent ORR/OER electrocatalytic performance caused by the active sites originated from the Co_4O_4 cubane subunits [58,59].

Perovskite oxides (ABO_3) are also promising bifunctional ORR/OER catalyst in alkaline electrolytes because their composition can be finely tuned by substituting A and B components by different metal cations [4]. In general, A-site mainly is responsible for oxygen adsorption capability, and B-site typically affects the activity of the adsorbed oxygen. Yamada et al. synthesized quadruple $CaMn_7O_{12}$ and $LaMn_7O_{12}$ perovskites which resulted in high OER onset potentials (up to ≈0.9 V vs RHE) and OER overpotential (η) values (0.27 and 0.30 V, respectively) comparable to that of RuO_2 (η = 0.31 V) [60].

1.2.2 Carbon-based composites

High-surface-area carbon is widely used material in preparation of non-precious catalysts for energy-related applications. The superiority of nanostructured carbon material is due to its high conductivity and high surface area [61]. Rational design of carbon-based nano-materials with multiple active centers is one of the most promising ways to prepare multifunctional catalysts for the ORR/OER. Therefore, heteroatom-doped carbon (preferably nitrogen-doped carbon (C-N)), and nitrogen and transition metal “co-doped” carbon (M-N-C, M = Fe or/and Co) composites have been widely investigated in recent years [62]. There are

three different reasons why nitrogen is preferred heteroatom as a doping agent. Firstly, if one carbon atom is replaced with one nitrogen in the carbon network then the total amount of electrons can be adjusted to one electron at a time. Secondly, nitrogen has a similar atomic radius with carbon. Thirdly, doping with nitrogen can cause an electronic modification of the carbon structures, allowing the use of these carbon-nitrogen structures in further major electronic applications [62]. Recently, Wang and coworkers synthesized hollow frameworks of N-doped carbon nanotubes (NCNTs) using ZIF-67 as a precursor [63]. Co nanoparticles in NCNTFs were removed by acid treatment and the obtained metal-free NCNTFs exhibited higher electrocatalytic activity and stability for ORR and OER than commercial Pt/C [63]. Porous N-doped carbon microtube (NCMT) sponge was prepared by pyrolyzing facial cotton and obtained micron-scale hollow core and well-graphitized porous structure of NCMT sponge exhibited excellent electrocatalytic activity for ORR and OER with ΔE value of 0.63 V vs RHE [64].

By optimizing transition metal and heteroatom precursors, different carbonization conditions, degree of graphitization, it is possible to finely tune the porosity of material and oxidation state of the metal. Zheng et al. obtained highly effective ORR/OER Co-N-C electrocatalyst by carbonizing bimetallic CoZn-MOFs precursor [65]. The highest ORR (comparable to Pt/C) and OER (E_{10} = 1.67 V vs RHE, better than lrO_2/C of 1.72 V) activities were obtained after carbonization precursors at 1100 °C. Electrochemically durable Co-N-C composite was prepared by carbonization of ZIF-67/polypyrrole nanofiber network rooted on carbon cloth exhibited low overpotential of 0.31 V at 10 mA cm^{-2} for OER, and a half-wave potential of 0.8 V for ORR [66]. Due to enhanced electrical conductivity, facilitated mass transport, improved dispersion, and exposure of catalytic sites, transition metals supported on nitrogen-doped carbonaceous materials (such as carbon nanotubes, graphene and porous carbon) have shown superior electrocatalytic activity [31]. When transition metal active species, such as metallic nanoparticles, metal oxide, and metal phosphides, are combined with carbon materials (*e.g.* graphene and carbon nanotubes), they practically always show promising electrocatalytic activities for potential applications in energy conversion and storage based technologies [31].

1.3 Shungite

Shungite is a natural carbon-rich amorphous mineraloid that is mainly found in Karelia, Russia, and its total reserve is estimated more than 250 gigatons [67]. Shungite has a heterogeneous structure in which carbon exists in irregularly distributed nanosized globules made of curved graphene layers [68,69]. Shungite has high electrical conductivity, and a relatively high specific surface area (200 to 400 m^2 g^{-1}) [70]. The basic structure of shungite offers a strong reason for considering this material as a viable alternative to synthetic graphene in various applications. Since, few-layer graphene platelets require high volume production, today, one of the main challenges is to develop technologies for expanding the preparation process while preserving properties [71]. A detailed experimental study confirmed that shungite is composed of spherical bundles of curved graphene layers, which makes shungite a great source of nature-derived carbon nanomaterials [72]. Based on carbon content shungite is classified into 5 types: I) 84-89 %, II) 42-84 %, III) 30-37 %, IV) 15-20 %, V) 3-6 % [70]. In addition to carbon, raw shungite also contains pyrite, quartz, mica, carbonates, chlorites, zircon, and other minerals [73]. Due to its abundance and unique properties, shungite has a great perspective for application in technology and medicine [74]. Today, shungite is utilized in water purification and treatment systems, as a filler for various purpose composite materials and in other industrial applications [72]. Shungite powder is very popular in alternative medicine and is often used for sanitary and therapeutic purposes due to its antiseptic properties [72].

Moreover, shungite shows exclusive electrochemical properties due to its high conductivity and resistance to harsh electrochemical conditions [75]. Gusmão et al. tested the electrocatalytic activity of raw shungite powder toward OER and HER in 1.0 M KOH solution [69]. As a result, due to the different impurities present in shungite, it outperformed other tested carbon materials such as carbon black, carbon nanotubes, fullerene, and glassy carbon [69]. The current density of 10 mA cm^{-2} on shungite modified electrodes was achieved at 1.09 V vs RHE [69]. Shungite's catalytic effect on OER can be influenced by the presence of different metals including transition metals in the composition of raw shungite. Chou et al. introduced carbon-rich shungite as an effective electrode material for Li-ion batteries [67]. Resulted energy density exceeded the one obtained for graphite, which makes shungite a promising candidate material for high energy density electrode in Li-ion batteries.

İn this bachelor thesis, shungite-based catalyst materials were prepared and their electrocatalytic behavior was evaluated toward both oxygen reduction and oxygen evolution reactions.

2 THE AIMS OF THE THESIS

The aims of this thesis are:

- Aim 1. To define the optimal purification protocol for raw shungite material.
- Aim 2. To dope the processed shungite powder with nitrogen and transition metals.
- Aim 3. To evaluate the electrocatalytic activity of shungite-based catalysts toward OER and ORR in 0.1 M KOH solution.
- Aim 4. To compare the electrochemical activity of prepared shungite-based catalysts with commercial benchmark catalysts.
- Aim 5. To explore the electrochemical stability of the most promising shungite-based catalysts toward ORR and OER.

3 EXPERIMENTAL PART

3.1 MATERIALS AND METHODS

3.1.1 Materials

Shungite powder used in this work was purchased from Strecker UG (Würzburg, Germany). Dicyandiamide (DCDA), melamine (purity 99 %), $CoCl_2$ (purity 97 %), $Fe(OAc)_2$ (purity 95 %), concentrated nitric (HNO_3) and hydrofluoric (HF) acids, 2-propanol (purity 99.8 %) and polyvinylpyrrolidone (PVP) were purchased from Aldrich. The electrolyte solution was prepared daily using Milli-Q water and KOH pellets (p.a. quality, Merck) and saturated with pure O_2 (99.999%, AGA) and with Ar gas (99.999%, AGA). Commercial 20 wt.% Pt/C (E-TEK) and 99.9 % RuO_2 (Alfa Aesar) were used as electrochemical benchmark catalysts for ORR and OER, respectively. Nafion ionomer dispersion (5 wt %, Alfa Aesar) was used for the preparation of catalyst inks. All chemicals and reagents (except shungite powder) were used without further purification.

3.1.2 Purification of shungite material

In this work, a systematic morphological examination was performed in order to define the optimal purification protocol for raw shungite material (SH_1). Due to its geological nature, unprocessed shungite powder typically contains different phases, such as amorphous carbon, silica, iron pyrite, and other minerals. Impurities, such as transition metals can have a strong effect on the electrocatalytic activity of shungite, even if they are in the form of traces [69]. In order to adequately evaluate the electrocatalytic behavior of shungite carbon, it is necessary to perform its chemical purification and make the composition of shungite more homogeneous. First, SH_1 was washed with plenty of deionized water and 2-propanol using vacuum filtering and subsequent drying in air. The resulting material was designated as SH_2. For more comprehensive purification SH_1 was acid-treated in the mixture of concentrated hydrofluoric and nitric acids (1:1 HF/HNO_3) by stirring for 12 h at room temperature, following by filtering with water and 2-propanol (SH_3) [71].

3.1.3 Preparation of shungite-based catalysts

SH_3 was doped with nitrogen, cobalt, and iron. Two different nitrogen sources such as melamine (MEL) and dicyandiamide (DCDA) were used for this purpose. For doping, 100 mg of shungite powder, 2 g of nitrogen source and a certain amount of metal precursors (4 mg of $Fe(OAc)_2$ and 10 mg of $CoCl_2$) were suspended in 2-propanol and 10 mg of PVP was

added to each suspension. Doping suspensions were sonicated for 2h at room temperature and dried overnight at 60 ^{o}C. After evaporation of the solvent, materials were transferred into the ceramic boats and pyrolyzed in a quartz tube furnace at 800 ^{o}C for 2h under N_2 gas flow. As a result, six different shungite samples were prepared and labeled according to the elements they were doped with SH_3DCDA-Co, SH_3DCDA-Fe, SH_3DCDA-Co-Fe, SH_3MEL-Co, SH_3MEL-Fe, SH_3MEL-Co-Fe.

3.1.4 Physical characterization

The microstructure of prepared samples was investigated by high-resolution transmission electron microscopy (HR-TEM, JEOL 2200FS FEG at 80kV). Catalyst powders were dispersed in 2-propanol using sonication and drop-casted onto amorphous carbon film with the copper grid. The scanning electron microscopy (SEM) measurement were carried out using a scanning electron microscope (HeliosTM NanoLab 600, FEI) equipped with an energy-dispersive X-ray spectroscope (INCA Energy 350, Oxford Instruments). Brunauer–Emmett–Teller (BET) surface area was measured with NOVAtouch LX2 (Quantachrome Instrument). Prior to measurements all samples were degassed overnight at 200 ^{o}C. Crystallinity and phase purity of the samples was examined by powder X-ray diffraction (XRD) analysis (SmartLab, Rigaku). Raman spectra were recorded by Horiba's LabRam HR800 spectrometer with a laser line of 532 nm, which was focused on the sample with a spot size of 5 μm.

3.1.5 Electrochemical measurements

The rotating-disk electrode (RDE) method was used to investigate the performance of prepared electrocatalysts toward ORR/OER. Major performance indicators of reaction kinetics were recorded using cyclic voltammetry (CV) by loading electrocatalyst onto the working electrode (Teflon-embedded glassy carbon (GC) disc with a geometric area of 0.126 cm^2). The RDE measurements were performed by EDI101 rotating disk electrode system and CTV101 speed control unit (Radiometer) in a typical electrochemical 3-electrode cell connected to an electrochemical workstation Autolab potentiostat/galvanostat PGSTAT30 (Eco Chemie B.V.). The counter electrode was GC rod and all potentials were measured against a reversible hydrogen electrode (RHE) connected to the cell via a Luggin capillary.

Prior to modification, GC disks of the working electrodes were polished to a mirror finish with 1 and 0.3 μm alumina slurries (Buehler) and sonicated in 2-propanol and Milli-Q water for 5 min to remove polishing residues.

The catalyst ink was prepared by dispersing the mixture of 5 mg of catalyst in 1 mL of 0.05 wt.% Nafion solution in 2-propanol with the aid of sonication. 4 μL of the catalyst suspension was pipetted onto the electrode. The catalyst loading was 0.153 μg cm^{-2}. Comparison experiments were performed with commercial 20 wt% Pt/C (loading 0.115 μg_{Pt} cm^{-2}) and 99.9 % RuO_2 (loading 0.120 μg cm^{-2}).

Main kinetic parameters of ORR, such as onset potential (E_{onset}), half-wave potential ($E_{1/2}$), diffusion-limited current density (j_d), number of transferred electrons (n), kinetic-limiting current density (j_k) and Tafel slopes were carefully extracted from measured polarization curves.[76] The electrocatalytic properties of prepared materials were evaluated using the Koutecky-Levich (K-L) equation [77]:

$$\frac{1}{j} = \frac{1}{j_k} + \frac{1}{j_d} = -\frac{1}{nFkC_{O_2}^b} - \frac{1}{0.62nFD_{O_2}^{2/3}v^{-1/6}C_{O_2}^b\omega^{1/2}} \quad (11)$$

where j is the overall measured current density and j_k is the kinetic current density, j_d represents the diffusion-limited current density, F is the Faraday constant (96,485 C mol^{-1}), k denotes the rate constant for electrochemical reduction of oxygen, $C_{O_2}^b$ is the concentration of O_2 in the bulk of 0.1 M KOH solution (1.2×10^{-6} mol cm^{-3}) [78], D_{O_2} denotes the diffusion coefficient of O_2 (1.9×10^{-5} cm^2 s^{-1}) [78], v is the kinematic viscosity of the solution (0.01 cm^2 s^{-1}) [79] and ω is the rotation rate of the electrode (rad s^{-1}).

The chronoamperometry measurements were conducted by holding the rotating electrodes at a constant potential of 0.75 (for ORR) and 1.6 V vs. RHE (for OER) and lasted for 10,000 seconds in total.

All electrochemical experiments were performed at room temperature (23 ± 1 °C).

3.2 RESULTS AND DISCUSSION

3.2.1 Morphological characterization

As-received and processed shungite samples were first analyzed by scanning electron microscopy to evaluate the surface morphology and elemental composition. Fig.1 presents SEM images of shungite samples evidencing the presence of micro-clusters that are composed of multilayer structures. All the samples exhibited hierarchical porous structure with a high amount of interconnected graphene-like sheets. SH_1 sample exhibits high inhomoge-

neity due to the presence of a high amount of different phases. According to SEM examination accompanied by energy-dispersive X-ray spectroscopy (EDS) analysis, as-received shungite SH_1 contained 44 wt. % of carbon. Acid-washing yielded SH_3 with a carbon content of 88 at. %. Based on the EDS results the shungite material used in this work can be classified as type II shungite.

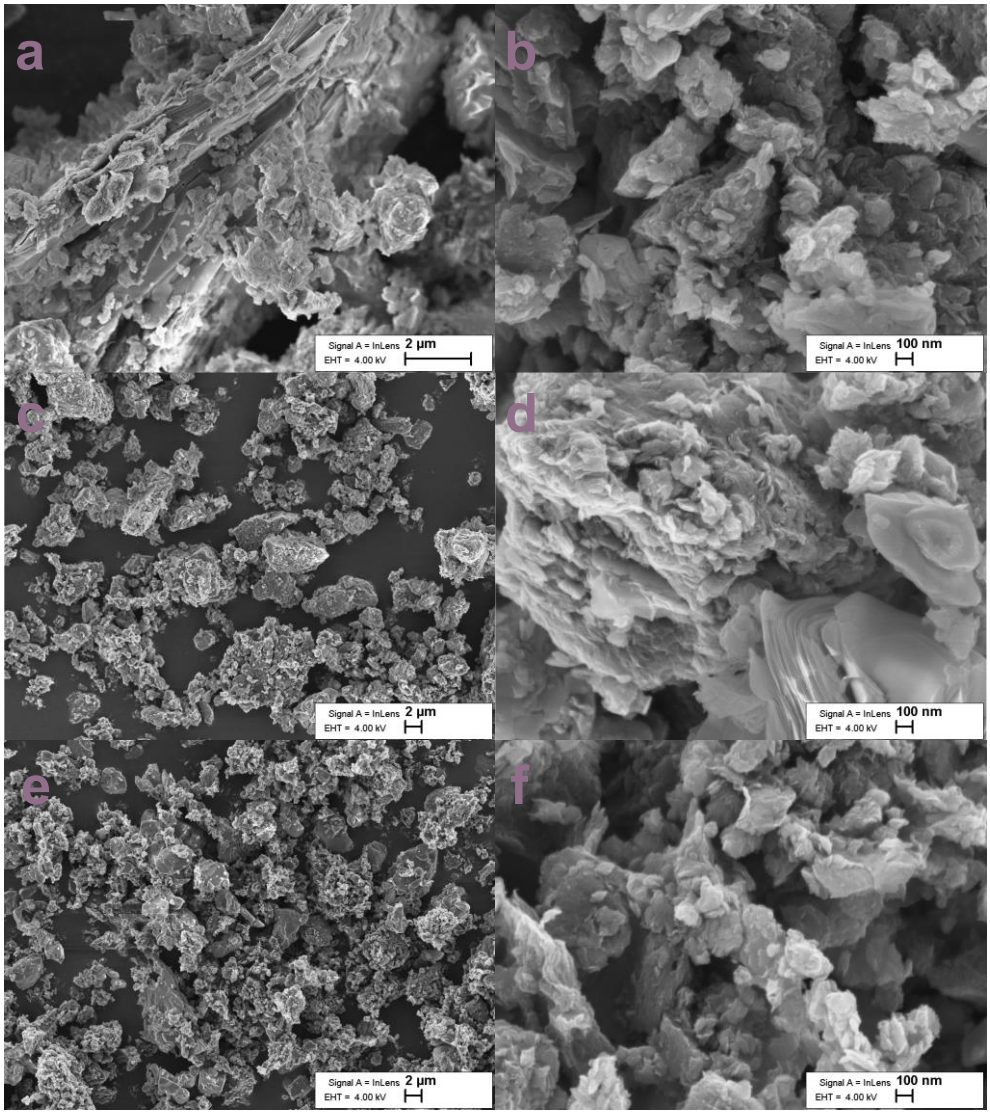

Figure 1. SEM micrographs of (a,b) as-received SH_1 and processed (c,d) SH_2 and (e,f) SH_3 samples at different magnification.

Furthermore, Fig. 2 shows TEM images of shungite before (a) and after (b,c) purification. Pristine shungite material forms an amorphous structure with the presence of additional phases. As confirmed by EDX analysis (Fig. 2d) non-processed shungite material contained a high amount of amorphous carbon, silica, iron, alumina, and sulfur impurities. Washing with water helps to get rid of amorphous carbon, also to wash out iron and sulfur compounds, which probably exist in the form of iron sulfite (Fig. 2e, confirmed later by XRD). After

acid-treatment, an ordered stacking of graphitic layers is observed (Fig. 2c) and the EDX spectrum confirms, that acid-leaching was very effective to remove all impurities (Fig. 2f), including silica and pyrite, yielding graphene-like sheets with high purity. As a result, we obtained clean carbon material which was further used as a support for ORR/OER catalysts.

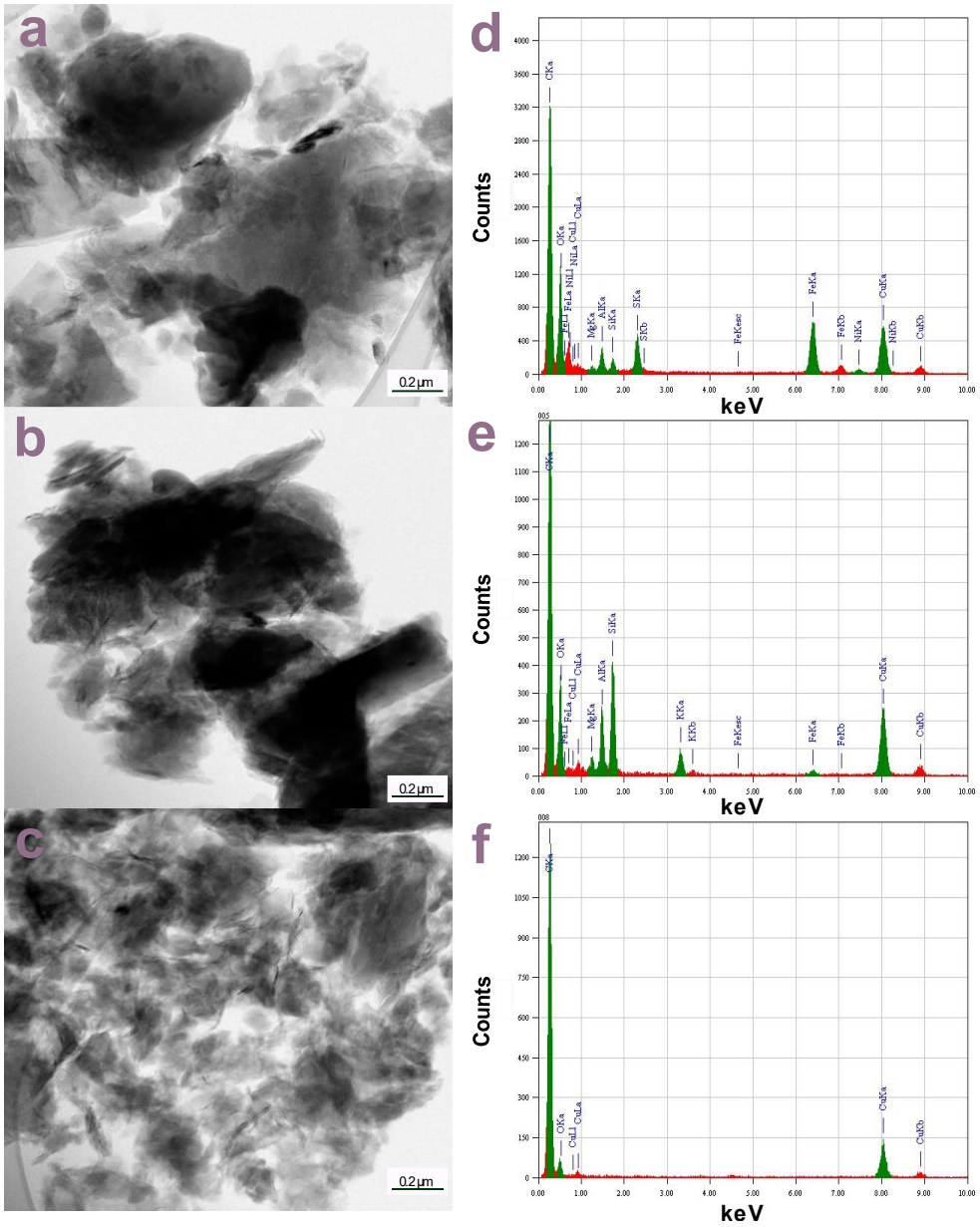

Figure 2. TEM images (a, b and c), and EDX spectrum (d, e and f), of $SH_{1\text{-}3}$ materials.

After doping of SH_3 with singe iron/cobalt metals, some single unevenly distributed metal particles were observed (Fig. S1). In contrast, the bimetallic system exibites more homogeneous distribution of nanoparticles (Fig. 3a) with a mean diameter of 29±9 nm. In order to thoroughly investigate the structural features of prepared bimetallic systems, high-resolution TEM (HRTEM) measurements were performed and presented in Fig. 3. HRTEM image of

SH_3DCDA-Co-Fe shows a typical particle present in the structure of the catalyst. The distribution of iron and cobalt metal within the particle can be clearly seen due to the difference in color intensity. Area with higher intensity is attributed to iron and is with lighter intensity corresponds to cobalt metal. It is also visible that the catalyst particles are surrounded by several graphitic carbon layers. The EDX elemental mapping of SH_3DCDA-Co-Fe indicates a homogeneous distribution of C, N, Fe, and Co atoms in the STEM image (see Fig. 3e). According to EDX spectrum, the Fe:Co ratio in the particle was 20:80 at.%.

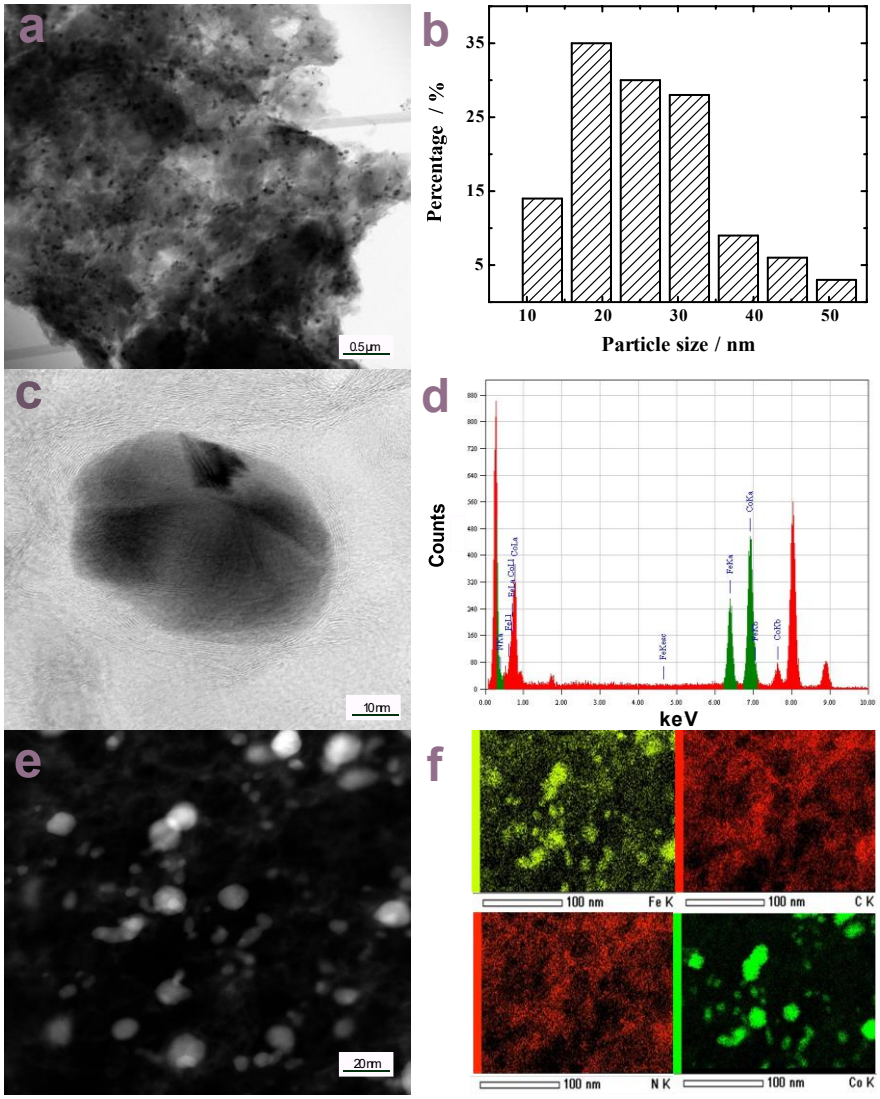

Figure 3. (a) TEM and (b) HRTEM image of SH_3DCDACoFe catalyst material; (b) statistical histogram of particle-diameters; (e) STEM image and (f) corresponding element mappings of SH_3DCDACoFe.

Since both the ORR and OER are heterogeneous reactions, the specific surface area is of great importance and all samples prepared in this work were examined by the dinitrogen adsorption-desorption analysis to ascertain their porosity. Brunauer-Emmett-Teller (BET)

surface areas of shungite-based samples were calculated and summarized in Table 1. The BET surface area (S_{BET}) of raw shungite powder was calculated to be ca. 102 m^2g^{-1}. Specific surface area values decrease slightly after purification of shungite. The S_{BET} of SH_3MEL-Fe reaches up to 127 m^2 g^{-1}, nevertheless, it remains almost unchanged for bimetallic powders. According to Fig. 4, all materials in this study had similar pore diameter distribution with a typical pore size of 3-5 nm.

Table 1. Specific surface area and porosity of shungite-based materials determined from dinitrogen physisorption analysis.

Catalyst	S_{BET} (m^2g^{-1})	S_{DFT} (m^2g^{-1})	V_{tot} (cm^3g^{-1})	V_{μ} (cm^3g^{-1})
SH_1	101	70	0.17	0
SH_2	102	74	0.17	0
SH_3	94	70	0.15	0
SH_3MEL-Fe	127	84	0.18	0.01
SH_3DCDA-Co	47	25	0.08	0
SH_3MEL-Co	69	44	0.11	0.01
SH_3DCDA-Co-Fe	97	66	0.13	0.02
SH_3MEL-Co-Fe	83	55	0.13	0.01

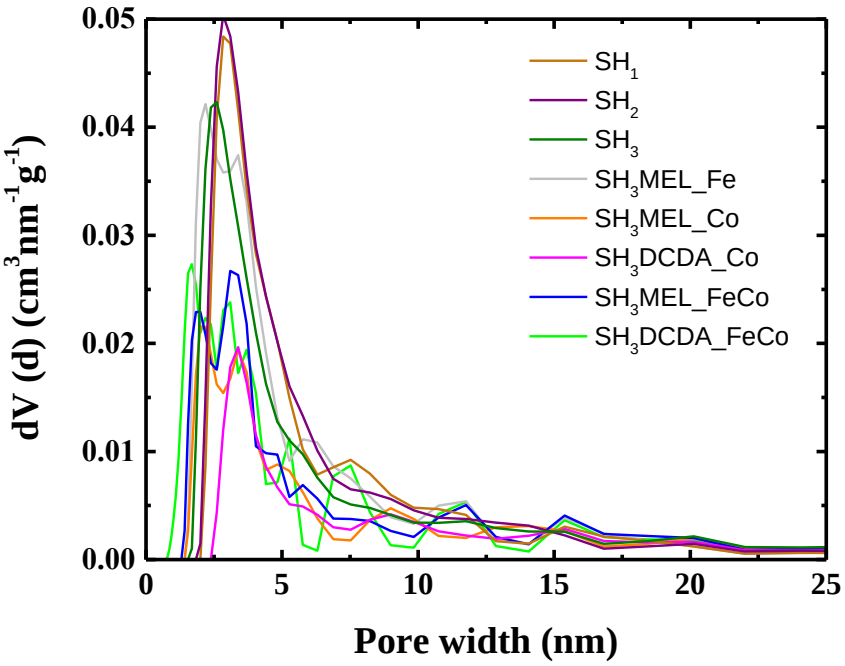

Figure 4. Pore size distribution of prepared materials.

The structure and composition of the samples were further investigated by X-ray diffraction analysis. Fig. 5a presents a typical diffraction pattern obtained for all shungite-based samples. According to the XRD peaks, carbon components are described as models of graphite–2H (hexagonal, 2-layer structure). There is also a possible mix of both graphite – 3R structure and graphite – 2H structure (42-45° 2θ). In SH_1 and SH_2, the peak at a 45° 2θ indicates the presence of coarse-grained graphite. Other peaks of graphite are overlapping with quartz. The small amount of SiO_2 as mineral quartz is present in all samples. Raw shungite sample contains a high amount of pyrite (FeS) which disappears after treatment with the acid mixture. Micas are described in the models with two different minerals just because some bigger flakes of mica are giving a sharp basal peak in top of the more diffuse peak of fine mica between 8 and 9° 2θ and around 18° 2θ. Furthermore, the addition of Co alone does not show up any difference in XRD pattern, while the addition of Fe alone alters the structure of carbon in a very interesting way. The highest peak (0 0 2) of graphite is shifting from the d value of 3.36 Å to 3.26 Å and the new peak arises at 6.8 Å. The addition of Co and Fe together raised two peaks at about 44-46° 2θ. The same interesting Fe peak can be noticed in the bimetallic sample as well.

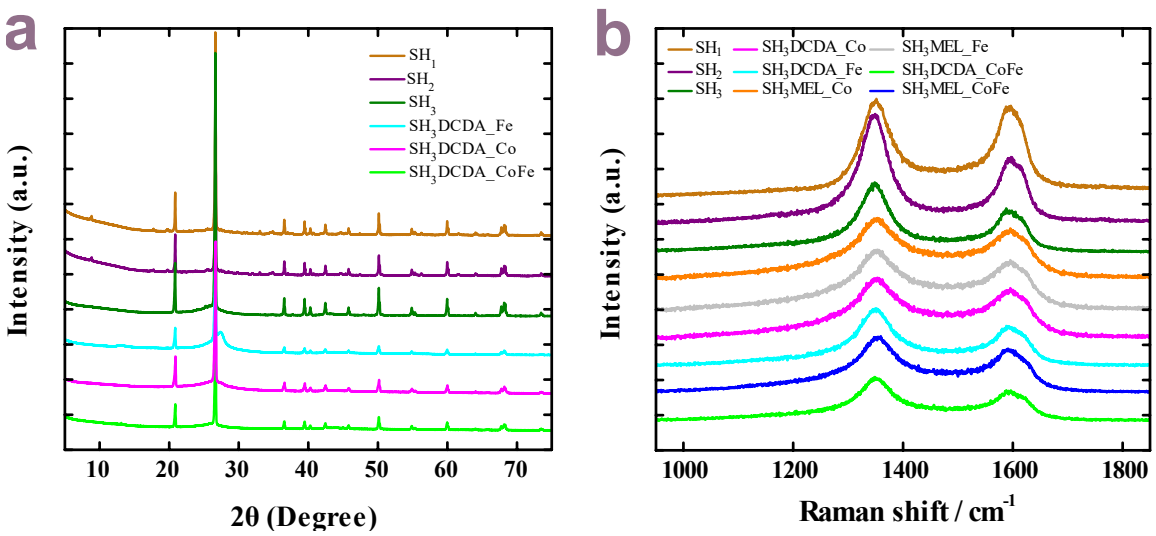

Figure 5. (a) XRD patterns of as-received, purified, and doped shungite powders; (b) Raman spectra of all shungite-based catalysts.

All shungite samples prepared in this study were explored by Raman spectroscopy. Fig. 5b compares the Raman spectra of prepared samples in the frequency range from 1000 to 1800 cm^{-1}. In the spectrum of amorphous carbon typically two peaks are observed – G (graphite) with the wave frequency at about 1560 cm^{-1} and D (diamond) at frequency of 1350 cm^{-1}, which corresponds to sp^2 bonds. An estimate of the total structural order in the carbon sample is given by the ratio of $Intensity_{Dband}$:$Intensity_{Gband}$ (I_D/I_G). The I_D/I_G ratio of SH_1, SH_2, SH_3, SH_3DCDA-Co, SH_3DCDA-Fe, SH_3DCDA-CoFe, SH_3MEL-Co, SH_3MEL-Fe, SH_3MEL-Co-Fe materials were 2.37, 2.31, 2.24, 2.65, 2.23, 2.37, 2.73, 1.87 and 2.38, respectively. These ratios can be used for comparison of the degree of defects and disorders of the 2D sp^2 carbon [80]. For all samples the intensity of D peaks are higher than G peaks, suggesting the higher concentration of sp^3 carbon content thus graphitic structure with a certain amount of disorder.

3.2.2 Electrochemical measurements

The electrocatalytic behavior of all materials in this work was first examined by cyclic voltammetry (CV) measurements in argon-saturated 0.1 M KOH solution. CV curves were recorded for as-received and purified shungite (Fig. 6a) and compared to CV curves obtained for doped shungite samples (Fig. 6b). As shown in Fig. 6a, SH_1 and SH_2 have similar surface oxidation peaks at about 0.3 V vs RHE, after acid-treatment, no obvious redox peaks are observed, evidencing the absence of electrocatalytic sites on the surface of SH_3 material.

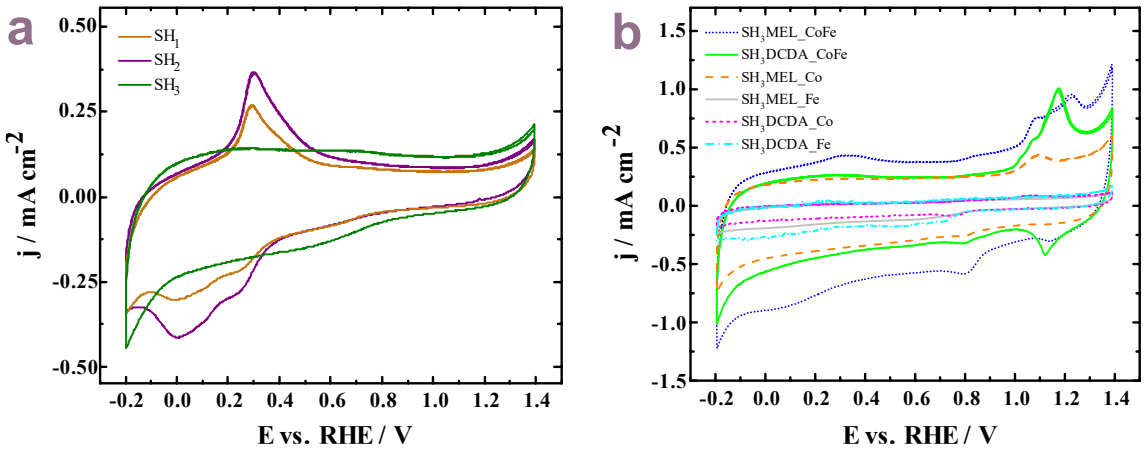

Figure 6. Cyclic voltammetry curves for (a) undoped shungite and (b) all the shungite-based powders modified GC electrodes in Ar-saturated 0.1 M KOH, scan rate 50 mV s^{-1}.

RDE measurements in O_2-saturated electrolytes were further used to investigate the ORR kinetics of prepared shungite-based catalysts. The background current was measured in O_2-free electrolyte at identical scan rate and was subtracted from the RDE data. The ORR polarization curves recorded at a single rotation rate of 1600 rpm and a scan rate of 10 mV s^{-1} are summarized in Fig. 7a. For the sake of comparison, the ORR on commercial Pt/C electrocatalyst was also examined in identical conditions. Each catalyst was tested at least three times to warrant good reproducibility. The ORR activity of raw and treated shungite alone is also presented in Fig. 7a. The diffusion-limited current density of Pt/C, SH_3DCDA-Co-Fe, SH_3MEL-Co-Fe, and SH_3MEL-Co was –6.17, –4.49, –6.34 and -5.61 mA cm^{-2}, respectively. The highest onset potential (E_{onset}) of 0.95 V and half-wave potential ($E_{1/2}$) of 0.80 V were observed for SH_3MEL-Co-Fe, which is very close to the commercial Pt/C (1.00 and 0.85 V vs. RHE, respectively). These results suggest that oxygen is more easily reduced on the SH_3MEL-Co-Fe catalyst. The detailed RDE characterizations of all the samples are presented in Fig. 7a and 8 and RDE full series for the bimetallic shungite-based catalyst are presented in Fig. 7b and 7d. Due to its unique hierarchically porous structure, shungite acts not only as a support but also as a facilitator of ORR promoting the transport of O_2 molecules to the catalytic sites.

The average number of electrons transferred per oxygen molecule (*n*) during the ORR was calculated using the Koutecky–Levich (K–L) equation in the potential range between 0.1 and 0.6 V vs. RHE (insets in Fig. 7c and 7e). Obtained values were close to 4 for almost all the doped shungite materials (Table 2). The lowest *n* value of 3.6 and 3.8 were found for SH_3DCDA-Co and SH_3DCDA-Co-Fe, respectively. These values indicate that shungite-supported catalysts are favorable for a 4-electron ORR pathway and the *n* values are very similar

to those obtained for the commercial Pt/C catalyst. The formation of hydrogen peroxide during the 2-electron ORR process is poisonous for catalyst materials and the 4-electron is desired in FC applications.

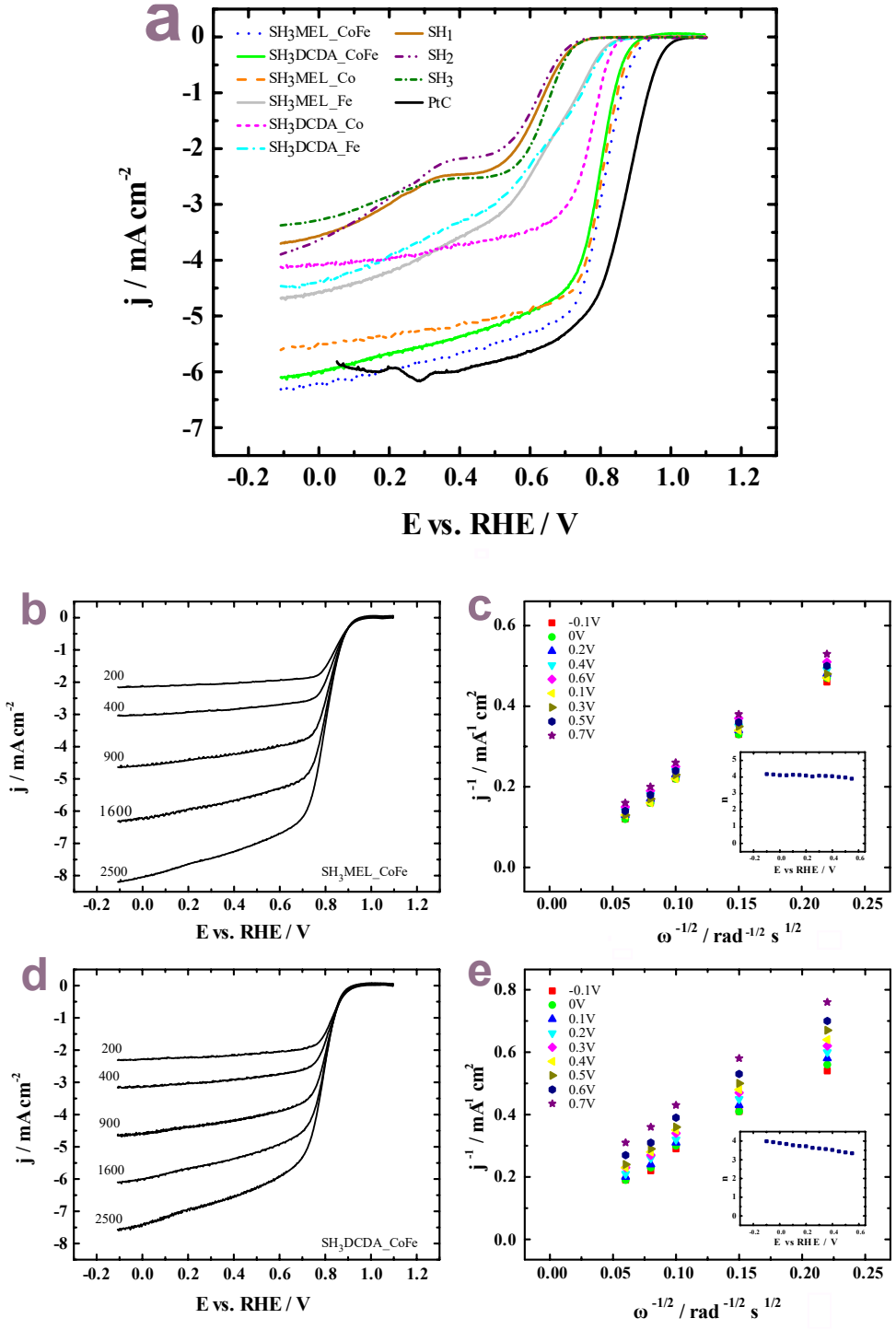

Figure 7. (a) Comparison of ORR polarization curves at 1600 rpm, scan rate v = 10 mV s^{-1}. (b,d) RDE polarization curves obtained for SH_3MEL-Co-Fe and SH_3DCDA-Co-Fe modified GC electrodes at different rotation rates in O_2 saturated 0.1 M KOH; (c,e) K-L plots, insets: *n* as a functional potential.

The performance of shungite-based catalysts was also examined toward OER in the Ar saturated 0.1 M KOH electrolyte. To obtain OER data the polarization RDE curves were measured from 1.0 to 1.8 V vs. RHE at a scan rate of 10 mV s^{-1} in O_2-saturated electrolyte. The electrode was rotated at 1600 rpm in order to avoid the detachment of the catalyst evolved by O_2 adhesion. Apart from the exceptional ORR activity, the bimetallic shungite-based catalysts also exhibited very good OER activity. Corresponding OER polarization curves obtained are shown in Fig. 8. Commercial RuO_2 electrocatalyst was also tested as a benchmark. Clearly, the SH_3MEL-Co-Fe and SH_3DCDA-Co-Fe catalysts exhibited much lower overpotential and a higher current density in the specified potential range compared to the commercial RuO_2 benchmark (Fig. 9).

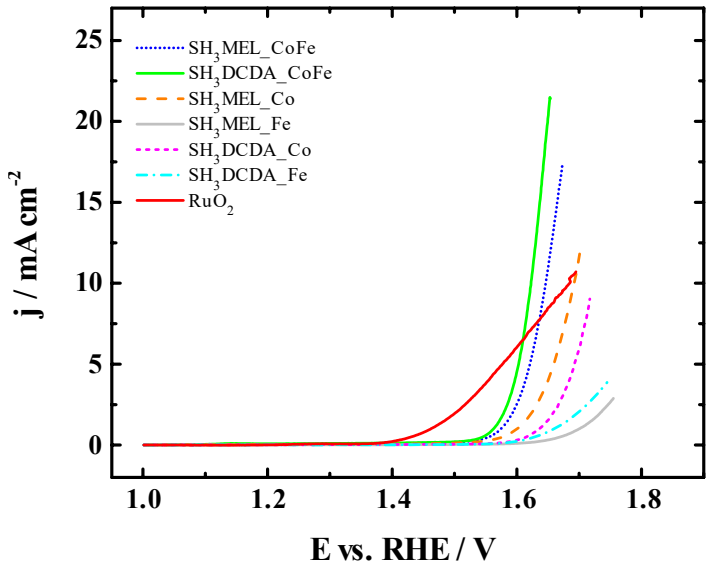

Figure 8. iR-corrected OER in Ar -saturated 0.1 M KOH

The overpotential values for SH_3DCDA-Co-Fe, SH_3MEL-Co-Fe, and commercial RuO_2 at a current density of 10 mA cm^{-2} were 0.39, 0.42, and 0.45 V, respectively (Fig. 9). The overpotential values obtained for bimetallic catalyst materials are outperforming the *state-of-the-art* RuO_2 catalyst. These results indicate that shungite-based bimetallic systems have superior OER electrocatalytic activity. Both single metal Fe-based catalysts showed poor OER response, indicating that Fe alone is not able to work as an active catalytic site for the OER. The excellent OER activity of bimetallic catalysts probably arises from their synergistic interaction affecting OER properties.

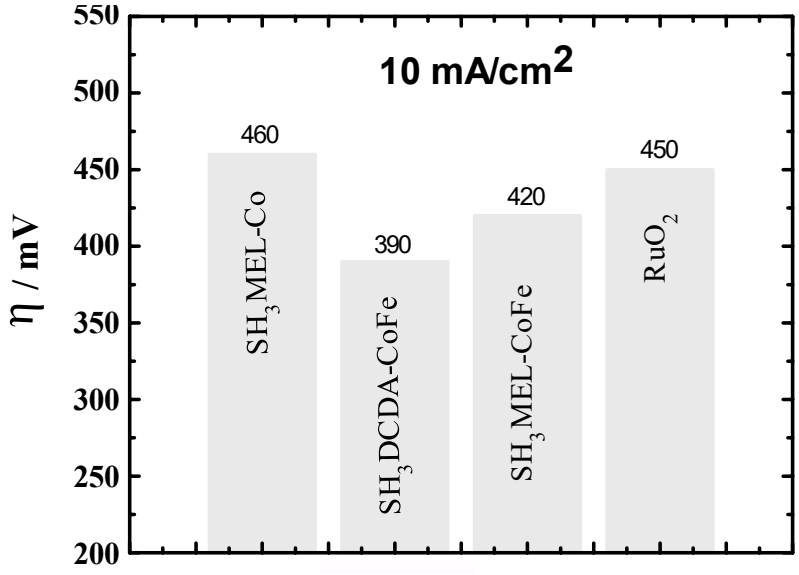

Figure 9. Bar plots of the OER overpotential.

The Tafel slopes derived from the ORR and OER polarization curves at 1600 rpm at a scan rate of 10 mV s^{-1} are shown in Fig. 10a and b. As shown in Fig. 10b, the OER Tafel plots for SH_3DCDA-Co-Fe exhibit a slope of 53 mV dec^{-1}, lower than that of the SH_3MEL-Co-Fe (74 mV dec^{-1}), SH_3DCDA-Fe (96 mV dec^{-1}), and RuO_2 (256 mV dec^{-1}) catalysts. SH_3DCDA-Co-Fe had the lowest Tafel slope value, which makes this material the most active OER electrocatalyst in this study.

The overall oxygen electrode bifunctional activity was evaluated by the difference in the potential (ΔE) between an ORR current density of −3 mA cm^{-2} ($E_{1/2}$) and an OER current density of 10 mA cm^{-2} (E_{10}) (Figure 10c) [4]:

$$\Delta E = E_{10} - E_{1/2} \qquad (12)$$

The main kinetic parameters obtained in this study are summarized in Table 2.

Table 2. Summary of electrocatalytic performance of all shungite-based catalysts.

Catalyst material	$E_{1/2}$ (V)	E_{onset} (V)	E_{10} (V)	ΔE (V)	n	η (V)
SH_1	-	0.77	-	-	3.2	-
SH_2	-	0.77	-	-	3.3	-
SH_3	-	0.78	-	-	2.5	-
SH_3DCDA-Fe	0.60	0.87	-	-	4.0	-
SH_3MEL-Fe	0.62	0.87	-	-	4.2	-
SH_3DCDA-Co	0.76	0.87	-	-	3.6	-
SH_3MEL-Co	0.80	0.93	1.69	0.89	4.0	0.46
SH_3DCDA-Co-Fe	0.78	0.92	1.62	0.84	3.8	0.39
SH_3MEL-Co-Fe	0.80	0.95	1.65	0.85	4.0	0.42
Pt/C	0.86	1.02	-	-	3.9	
RuO_2	-	-	1.68	-	-	0.45

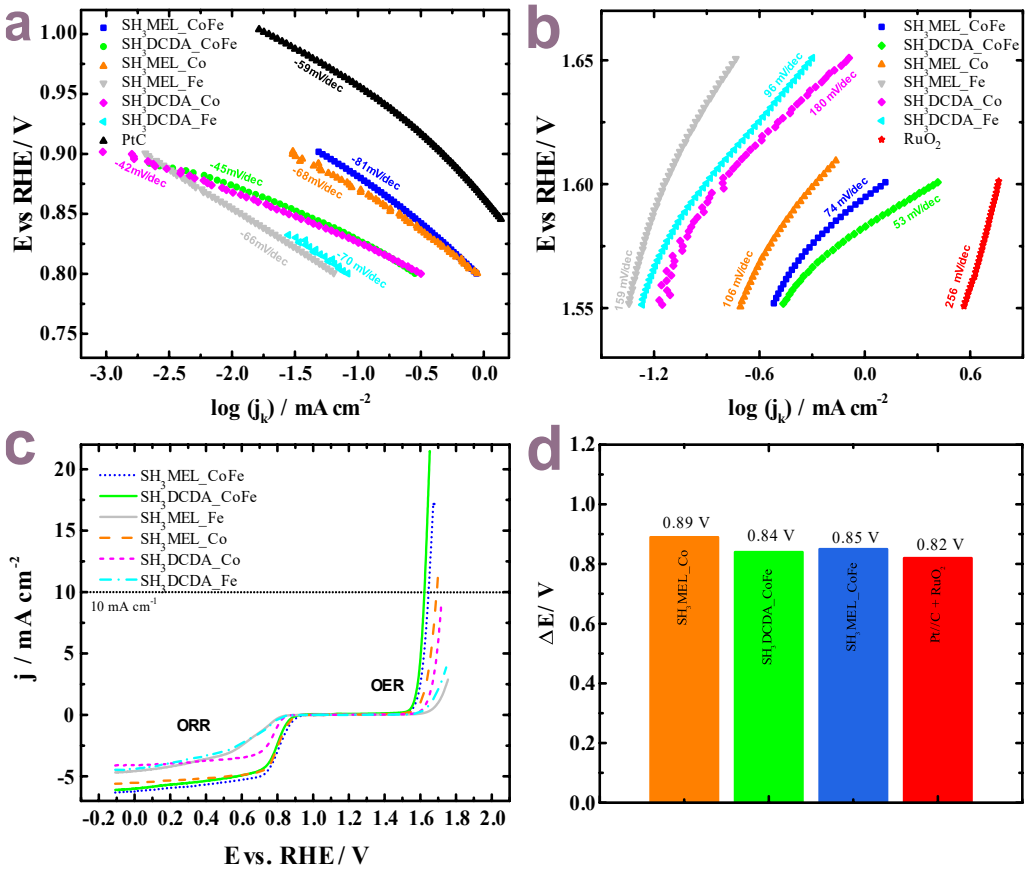

Figure 10. ORR (a) and OER (b) Tafel plots of the catalysts, (c) the overall oxygen polarization curves of shungite-based catalysts; (d) ΔE of samples SH_3MEL-Co, SH_3DCDA-Co-Fe, SH_3MEL-Co-Fe.

In order to compare the bifunctional oxygen electrocatalytic behaviour of SH_3DCDA-Co-Fe and SH_3MEL-Co-Fe with the recent developments, the major kinetic parameters (such as j_{10} and ΔE) were screened in recent publications on bifunctional electrocatalysts (Table S1).

The stability of SH_3DCDA-Co-Fe and SH_3MEL-Co-Fe as bifunctional catalysts were examined using the chronoamperometric method. The stability measurement for OER and ORR was conducted in Ar-saturated and O_2-saturated 0.1 M KOH solution, respectively. For ORR stability, the electrode was held at 0.75 V vs. RHE, while for OER stability, the potential was held at 1.6 V vs RHE during 10,000 s. As a result, SH_3DCDA-Co-Fe catalyst showed the best stability performance either in ORR or in OER by exceeding precious metal catalysts. SH_3DCDA-Co-Fe showed better electrocatalytic stability during both the ORR and OER than commercial Pt/C and RuO_2 catalysts after 10,000 s (Fig. 11a,b).

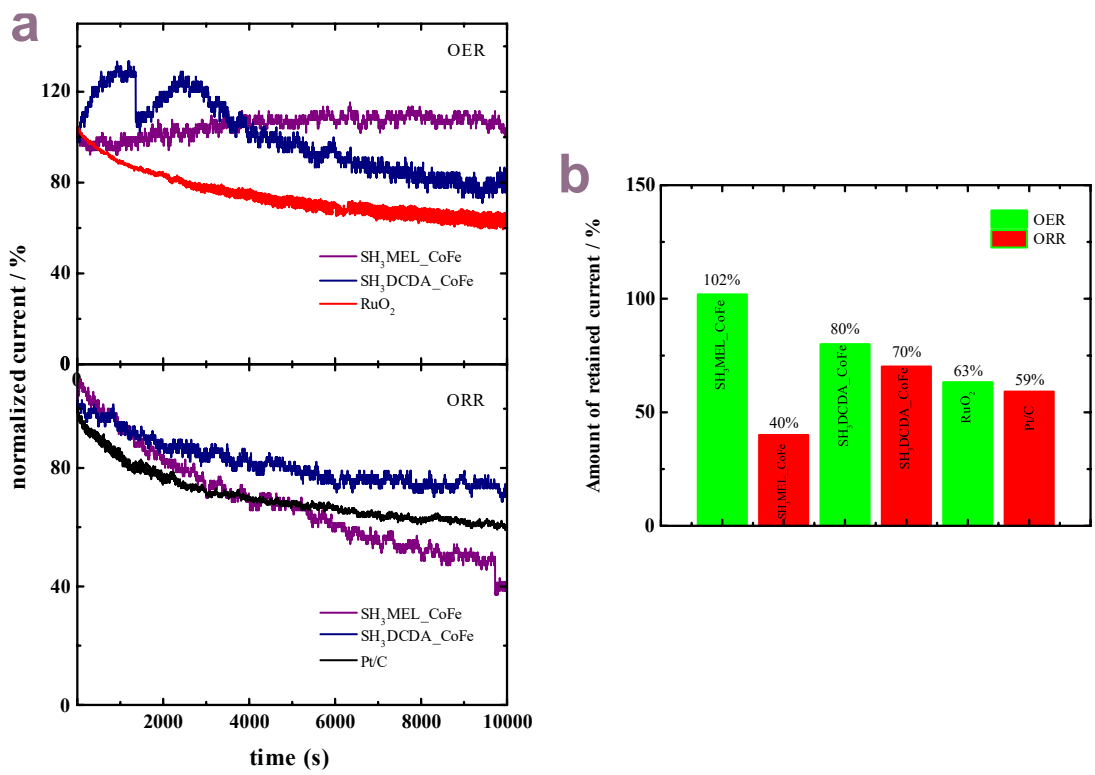

Figure 11. (a) Current-time chronoamperometry response for the ORR at 0.75 V and the OER at 1.60 V vs. RHE; (b) normalized current of the catalysts for the ORR and the OER after stability experiments.

M-N-C composites are widely reported as bifunctional catalysts. For example, Xiao et al. reported electrochemical activity of $FeCo_x$ alloy nanoparticles encapsulated in N-doped porous carbon/carbon nanotubes composites (FCx-NC/CNTs) in alkaline environment. As a result, $E_{1/2}$ (0.79 V), E_{onset} (0.9 V) and E_{10} (1.59 V) [81] , which is very close to the results obtained in this work for shungite supported bimetallic and Co catalysts. Similarly, Liu et al. synthesized transition metal nanoparticles (cobalt and iron) encapsulated in N-doped CNTs and bifunctional electrocatalyst activity ΔE for Co/N-CNTs and Fe/N-CNTs were 0.78 and 0.94, respectively [82]. Sun et al. reported *in – situ* synthesized Co_3O_4/NPC for oxygen electrode in alkaline medium. For ORR, it showed half-wave potential of 0.82 V which is close to the electrochemical performance of commercial SH_3MEL-Co-Fe (0.80 V), SH_3DCDA-Co-Fe (0.79 V), SH_3MEL-Co (0.80 V). For OER, the catalyst shows a low overpotential of 0.39 V at 10 mA cm^{-2} and the Tafel slope value is 45 mV dec^{-1} [83], which is very close to the observed OER Tafel plot in this study (SH_3DCDA-Co-Fe, 53 mV dec^{-1}).

Improved bifunctional oxygen activity is mainly the result of the fact that: firstly, shungite support provides better mass transport of O_2 within the structure of catalyst; secondly, due to rich source of N atoms melamine and DCDA increase nitrogen content in catalysts, and

the amount of nitrogen containing active sites on the carbon support. Thirdly, introduction of transition metal increases the ratio of C-N and M-N_x sites, which are responsible for good oxygen electrocatalytic activity.

It was confirmed that the composition of catalyst material plays a crucial role in the overall bifunctional activity, and materials with multiple electroactive sites are great candidates for efficient ORR/OER electrocatalysis. Catalyst materials consisting of multiple elements generally exhibit a synergistic effect, some centers are active toward ORR and others are beneficial for OER, hence lowering the overall overpotential [84].

SUMMARY

In this work, low-cost highly active shungite-based oxygen electrocatalyst materials were fabricated using simple and efficient strategy. The synergistic integration of cobalt and iron metals along with nitrogen endows shungite-based materials with a superior bifunctional electrocatalytic performance.

The composition and structure of as-received, and processed shungite was performed by combined use of several techniques (scanning electron microscopy, high-resolution transmission electron microscopy, BET, X-ray diffraction and Raman spectroscopy). The electrocatalytic behavior of prepared materials was investigated in alkaline electrolyte toward ORR and OER.

As a result, the purification of shungite with HF/HNO_3 acid mixture was very effective, and pure shungite material was obtained for further synthesis procedures. As expected, the doping of shungite with nitrogen, iron, and cobalt increased the electrocatalytic activity. Shungite-supported bimetallic catalysts showed remarkable bifunctional electrocatalytic activity by catalyzing ORR via 4-electron pathway and outperforming commercial RuO_2 benchmark in OER. Specifically, SH_3MEL-Co, SH_3MEL-Co-Fe, SH_3DCDA-Co-Fe demonstrated the highest electrochemical performance as bifunctional catalysts toward OER and ORR. The half-wave potentials of SH_3MEL-Co and SH_3MEL-Co-Fe catalysts were very close to the commercial Pt/C catalyst, while SH_3MEL-Co-Fe and SH_3DCDA-Co-Fe outperformed commercial RuO_2 catalyst by exhibiting lower overpotential and higher current density. Moreover, SH_3DCDA-Co-Fe showed the lowest Tafel slope value and the highest stability for both OER and ORR than other prepared catalysts. The prepared catalysts exhibited comparable combined ORR and OER overpotential to those obtained for commercial catalysts Pt/C (0.82 V) vs SH_3DCDA-Co-Fe (0.84 V). Commercial Pt/C and RuO_2 are active for only one of this two reactions, while shungite carbon supported catalyst material prepared in this thesis is highly active for both reactions.

ACKNOWLEDGEMENTS

I would like to express my sincere appreciation to my supervisor Dr. Nadezda Kongi for the research conduction opportunity, guidance, and support provided throughout the project.

I would like to thank Assoc. Prof. Kaido Tammeveski for his support.

I would like to thank Dr. Maike Käärik (UT) for the BET measurement, Dr. Jaan Aruväli (UT) for the XRD measurement, Dr. Pavel Starkov (TalTech) for SEM and Raman measurements and Dr. Hua Jiang (Aalto university) for HRTEM measurement in this work.

This work was supported by the Estonian Research Council grant (PSG250).

REFERENCES

[1] K. Ping, A. Braschinsky, M. Alam, R. Bhadoria, V. Mikli, A. Mere, J. Aruväli, P. Paiste, S. Vlassov, M. Kook, M. Rähn, V. Sammelselg, K. Tammeveski, N. Kongi, P. Starkov, Fused Hybrid Linkers for Metal–Organic Framework-Derived Bifunctional Oxygen Electrocatalysts, ACS Appl. Energy Mater. 3 (2020) 152–157.

[2] I.B. Volkova, M.V. Bogdanova, Petrology and genesis of Karelian shungite—high rank coal, Int. J. Coal Geol. 6 (1986) 369–379.

[3] M. Tahir, L. Pan, F. Idrees, X. Zhang, L. Wang, J.-J. Zou, Z.L. Wang, Electrocatalytic oxygen evolution reaction for energy conversion and storage: A comprehensive review, Nano Energy 37 (2017) 136–157.

[4] Z.-F. Huang, J. Wang, Y. Peng, C.-Y. Jung, A. Fisher, X. Wang, Design of Efficient Bifunctional Oxygen Reduction/Evolution Electrocatalyst: Recent Advances and Perspectives, Adv. Energy Mater. 7 (2017) 1700544.

[5] R. Cao, J.-S. Lee, M. Liu, J. Cho, Recent Progress in Non-Precious Catalysts for Metal-Air Batteries, Adv. Energy Mater. 2 (2012) 816–829.

[6] M.K. Debe, Electrocatalyst approaches and challenges for automotive fuel cells, Nature. 486 (2012) 43–51.

[7] J. Zhang, L. Dai, Nitrogen, Phosphorus, and Fluorine Tri-doped Graphene as a Multifunctional Catalyst for Self-Powered Electrochemical Water Splitting, Angew. Chem. Int. Ed. 55 (2016) 13296–13300.

[8] P.P. Patel, M.K. Datta, O.I. Velikokhatnyi, R. Kuruba, K. Damodaran, P. Jampani, B. Gattu, P.M. Shanthi, S.S. Damle, P.N. Kumta, Noble metal-free bifunctional oxygen evolution and oxygen reduction acidic media electro-catalysts, Sci. Rep. 6 (2016) 28367.

[9] Z.-P. Wu, X.F. Lu, S.-Q. Zang, X.W. (David) Lou, Non-Noble-Metal-Based Electrocatalysts toward the Oxygen Evolution Reaction, Adv. Funct. Mater. 30 (2020) 1910274.

[10] R. Ma, G. Lin, Y. Zhou, Q. Liu, T. Zhang, G. Shan, M. Yang, J. Wang, A review of oxygen reduction mechanisms for metal-free carbon-based electrocatalysts, Npj Comp. Mater. (2019).

[11] Z.-L. Wang, D. Xu, J.-J. Xu, X.-B. Zhang, Oxygen electrocatalysts in metal–air batteries: from aqueous to nonaqueous electrolytes, Chem. Soc. Rev. 43 (2014) 7746–7786.

[12] S. Zhao, D.-W. Wang, R. Amal, L. Dai, Carbon-Based Metal-Free Catalysts for Key Reactions Involved in Energy Conversion and Storage, Adv. Mater. 31 (2019) 1801526.

[13] E.S.F. Cardoso, G.V. Fortunato, I. Palm, E. Kibena-Põldsepp, A.S. Greco, J.L.R. Júnior, A. Kikas, M. Merisalu, V. Kisand, V. Sammelselg, K. Tammeveski, G. Maia, Effects of N and O groups for oxygen reduction reaction on one- and two-dimensional carbonaceous materials, Electrochim. Acta 344 (2020) 136052.

[14] C. Song, J. Zhang, Electrocatalytic Oxygen Reduction Reaction, in: J. Zhang (Ed.), PEM Fuel Cell Electrocatalysts and Catalyst Layers: Fundamentals and Applications, Springer, London, 2008: pp. 89–134.

[15] Y. Shao, Z. Jiang, Q. Zhang, J. Guan, Progress in Nonmetal-Doped Graphene Electrocatalysts for the Oxygen Reduction Reaction, ChemSusChem 12 (2019) 2133–2146.

[16] Y. Li, H. Dai, Recent advances in zinc–air batteries, Chem. Soc. Rev. 43 (2014) 5257–5275.

[17] L. Zhang, J. Zhang, D. Wilkinson, H. Wang, Progress in preparation of non-noble electrocatalysts for PEM fuel cell reactions, J. Power Sources 156 (2006) 171–182.

[18] N. Zamel, X. Li, Effect of contaminants on polymer electrolyte membrane fuel cells, Prog. Energy Comb. Sci. 37 (2011) 292–329.
[19] M. Bron, J. Radnik, M. Fieber-Erdmann, P. Bogdanoff, S. Fiechter, EXAFS, XPS and electrochemical studies on oxygen reduction catalysts obtained by heat treatment of iron phenanthroline complexes supported on high surface area carbon black, J. Electroanal. Chem. 535 (2002) 113–119.
[20] Proton Exchange Membrane Fuel Cells 7, The Electrochemical Society, 2007.
[21] L.-T. Song, Z.-Y. Wu, F. Zhou, H.-W. Liang, Z.-Y. Yu, S.-H. Yu, Sustainable Hydrothermal Carbonization Synthesis of Iron/Nitrogen-Doped Carbon Nanofiber Aerogels as Electrocatalysts for Oxygen Reduction, Small 12 (2016) 6398–6406.
[22] M. Li, T. Liu, L. Fan, X. Bo, L. Guo, Three-dimensional hierarchical meso/macroporous Fe/Co-nitrogen-doped carbon encapsulated FeCo alloy nanoparticles prepared without any template or surfactant: High-performance bifunctional oxygen electrodes, J. Alloys Comp. 686 (2016) 467–478.
[23] Y. Liu, J. Ruan, S. Sang, Z. Zhou, Q. Wu, Iron and nitrogen co-doped carbon derived from soybeans as efficient electro-catalysts for the oxygen reduction reaction, Electrochim. Acta 215 (2016) 388–397.
[24] J. Lilloja, E. Kibena-Põldsepp, A. Sarapuu, A. Kikas, V. Kisand, M. Käärik, M. Merisalu, A. Treshchalov, J. Leis, V. Sammelselg, Q. Wei, S. Holdcroft, K. Tammeveski, Nitrogen-doped carbide-derived carbon/carbon nanotube composites as cathode catalysts for anion exchange membrane fuel cell application, Appl. Catal. B: Environ. 272 (2020) 119012.
[25] R. Praats, M. Käärik, A. Kikas, V. Kisand, J. Aruväli, P. Paiste, M. Merisalu, J. Leis, V. Sammelselg, J.H. Zagal, S. Holdcroft, N. Nakashima, K. Tammeveski, Electrocatalytic oxygen reduction reaction on iron phthalocyanine-modified carbide-derived carbon/carbon nanotube composite electrocatalysts, Electrochim. Acta 334 (2020) 135575.
[26] R. Sibul, E. Kibena-Põldsepp, S. Ratso, M. Kook, M.T. Sougrati, M. Käärik, M. Merisalu, J. Aruväli, P. Paiste, A. Treshchalov, J. Leis, V. Kisand, V. Sammelselg, S. Holdcroft, F. Jaouen, K. Tammeveski, Iron- and Nitrogen-Doped Graphene-Based Catalysts for Fuel Cell Applications, ChemElectroChem. 7 (2020) 1739–1747.
[27] Y. Li, Q. Li, H. Wang, L. Zhang, D.P. Wilkinson, J. Zhang, Recent Progresses in Oxygen Reduction Reaction Electrocatalysts for Electrochemical Energy Applications, Electrochem. Energ. Rev. 2 (2019) 518–538.
[28] M. Shen, C. Wei, K. Ai, L. Lu, Transition metal–nitrogen–carbon nanostructured catalysts for the oxygen reduction reaction: From mechanistic insights to structural optimization, Nano Res. 10 (2017) 1449–1470.
[29] S. Ratso, M.T. Sougrati, M. Käärik, M. Merisalu, M. Rähn, V. Kisand, A. Kikas, P. Paiste, J. Leis, V. Sammelselg, F. Jaouen, K. Tammeveski, Effect of Ball-Milling on the Oxygen Reduction Reaction Activity of Iron and Nitrogen Co-doped Carbide-Derived Carbon Catalysts in Acid Media, ACS Appl. Energy Mater. 2 (2019) 7952–7962.
[30] S. Ratso, M. Käärik, M. Kook, P. Paiste, J. Aruväli, S. Vlassov, V. Kisand, J. Leis, A.M. Kannan, K. Tammeveski, High performance catalysts based on Fe/N co-doped carbide-derived carbon and carbon nanotube composites for oxygen reduction reaction in acid media, Int. J. Hydrogen Energy. 44 (2019) 12636–12648.
[31] S. Li, X. Hao, A. Abudula, G. Guan, Nanostructured Co-based bifunctional electrocatalysts for energy conversion and storage: current status and perspectives, J. Mater. Chem. A 7 (2019) 18674–18707.

[32] C. Feng, M.B. Faheem, J. Fu, Y. Xiao, C. Li, Y. Li, Fe-Based Electrocatalysts for Oxygen Evolution Reaction: Progress and Perspectives, ACS Catal. 10 (2020) 4019–4047.
[33] L.C. Seitz, C.F. Dickens, K. Nishio, Y. Hikita, J. Montoya, A. Doyle, C. Kirk, A. Vojvodic, H.Y. Hwang, J.K. Norskov, T.F. Jaramillo, A highly active and stable IrOx/SrIrO3 catalyst for the oxygen evolution reaction, Science 353 (2016) 1011–1014.
[34] Y. Pi, Q. Shao, P. Wang, J. Guo, X. Huang, General Formation of Monodisperse IrM (M = Ni, Co, Fe) Bimetallic Nanoclusters as Bifunctional Electrocatalysts for Acidic Overall Water Splitting, Adv. Funct. Mater. 27 (2017) 1700886.
[35] Y. Lin, Z. Tian, L. Zhang, J. Ma, Z. Jiang, B.J. Deibert, R. Ge, L. Chen, Chromium-ruthenium oxide solid solution electrocatalyst for highly efficient oxygen evolution reaction in acidic media, Nat. Commun. 10 (2019) 162.
[36] Y. Yao, S. Hu, W. Chen, Z.-Q. Huang, W. Wei, T. Yao, R. Liu, K. Zang, X. Wang, G. Wu, W. Yuan, T. Yuan, B. Zhu, W. Liu, Z. Li, D. He, Z. Xue, Y. Wang, X. Zheng, J. Dong, C.-R. Chang, Y. Chen, X. Hong, J. Luo, S. Wei, W.-X. Li, P. Strasser, Y. Wu, Y. Li, Engineering the electronic structure of single atom Ru sites via compressive strain boosts acidic water oxidation electrocatalysis, Nat. Catal. 2 (2019) 304–313.
[37] B. Zhang, X. Zheng, O. Voznyy, R. Comin, M. Bajdich, M. García-Melchor, L. Han, J. Xu, M. Liu, L. Zheng, F.P.G. de Arquer, C.T. Dinh, F. Fan, M. Yuan, E. Yassitepe, N. Chen, T. Regier, P. Liu, Y. Li, P.D. Luna, A. Janmohamed, H.L. Xin, H. Yang, A. Vojvodic, E.H. Sargent, Homogeneously dispersed multimetal oxygen-evolving catalysts, Science 352 (2016) 333–337.
[38] C. Roy, B. Sebok, S.B. Scott, E.M. Fiordaliso, J.E. Sørensen, A. Bodin, D.B. Trimarco, C.D. Damsgaard, P.C.K. Vesborg, O. Hansen, I.E.L. Stephens, J. Kibsgaard, I. Chorkendorff, Impact of nanoparticle size and lattice oxygen on water oxidation on NiFeO x H y, Nat. Catal. 1 (2018) 820–829.
[39] Y. Kuang, M.J. Kenney, Y. Meng, W.-H. Hung, Y. Liu, J.E. Huang, R. Prasanna, P. Li, Y. Li, L. Wang, M.-C. Lin, M.D. McGehee, X. Sun, H. Dai, Solar-driven, highly sustained splitting of seawater into hydrogen and oxygen fuels, Proc. Nat. Acad. Sci. USA 116 (2019) 6624–6629.
[40] F. Guo, Y. Wu, H. Chen, Y. Liu, L. Yang, X. Ai, X. Zou, High-performance oxygen evolution electrocatalysis by boronized metal sheets with self-functionalized surfaces, Energy Environ. Sci. 12 (2019) 684–692.
[41] T. Zhang, J. Du, P. Xi, C. Xu, Hybrids of Cobalt/Iron Phosphides Derived from Bimetal–Organic Frameworks as Highly Efficient Electrocatalysts for Oxygen Evolution Reaction, ACS Appl. Mater. Interfaces 9 (2017) 362–370.
[42] L. Trotochaud, J.K. Ranney, K.N. Williams, S.W. Boettcher, Solution-Cast Metal Oxide Thin Film Electrocatalysts for Oxygen Evolution, J. Am. Chem. Soc. 134 (2012) 17253–17261.
[43] H. Wang, H.-W. Lee, Y. Deng, Z. Lu, P.-C. Hsu, Y. Liu, D. Lin, Y. Cui, Bifunctional non-noble metal oxide nanoparticle electrocatalysts through lithium-induced conversion for overall water splitting, Nat. Commun. 6 (2015) 7261.
[44] X.-F. Lu, L.-F. Gu, J.-W. Wang, J.-X. Wu, P.-Q. Liao, G.-R. Li, Bimetal-Organic Framework Derived CoFe2O4/C Porous Hybrid Nanorod Arrays as High-Performance Electrocatalysts for Oxygen Evolution Reaction, Adv. Mater. 29 (2017) 1604437.

[45] X. Jia, Y. Zhao, G. Chen, L. Shang, R. Shi, X. Kang, G.I.N. Waterhouse, L.-Z. Wu, C.-H. Tung, T. Zhang, Ni3FeN Nanoparticles Derived from Ultrathin NiFe-Layered Double Hydroxide Nanosheets: An Efficient Overall Water Splitting Electrocatalyst, Adv. Energy Mater. 6 (2016) 1502585.
[46] Z. Tao, T. Wang, X. Wang, J. Zheng, X. Li, MOF-Derived Noble Metal Free Catalysts for Electrochemical Water Splitting, ACS Appl. Mater. Interfaces 8 (2016) 35390–35397.
[47] X. Chen, L. Yu, S. Wang, D. Deng, X. Bao, Highly active and stable single iron site confined in graphene nanosheets for oxygen reduction reaction, Nano Energy 32 (2017) 353–358.
[48] P. Chen, T. Zhou, L. Xing, K. Xu, Y. Tong, H. Xie, L. Zhang, W. Yan, W. Chu, C. Wu, Y. Xie, Atomically Dispersed Iron–Nitrogen Species as Electrocatalysts for Bifunctional Oxygen Evolution and Reduction Reactions, Angew. Chem. Int. Ed. 56 (2017) 610–614.
[49] J. Suntivich, K.J. May, H.A. Gasteiger, J.B. Goodenough, Y. Shao-Horn, A perovskite oxide optimized for oxygen evolution catalysis from molecular orbital principles, Science 334 (2011) 1383–1385.
[50] E. Fabbri, M. Nachtegaal, T. Binninger, X. Cheng, B.-J. Kim, J. Durst, F. Bozza, T. Graule, R. Schäublin, L. Wiles, M. Pertoso, N. Danilovic, K.E. Ayers, T.J. Schmidt, Dynamic surface self-reconstruction is the key of highly active perovskite nano-electrocatalysts for water splitting, Nat. Mater. 16 (2017) 925–931.
[51] J. Du, T. Zhang, J. Xing, C. Xu, Hierarchical porous Fe3O4/Co3S4 nanosheets as an efficient electrocatalyst for the oxygen evolution reaction, J. Mater. Chem. A 5 (2017) 9210–9216.
[52] X.F. Lu, Y. Chen, S. Wang, S. Gao, X.W. Lou, Interfacing Manganese Oxide and Cobalt in Porous Graphitic Carbon Polyhedrons Boosts Oxygen Electrocatalysis for Zn-Air Batteries, Adv. Mater. 31 (2019) 1902339.
[53] H. Osgood, S. Devaguptapu, H. Xu, J. Cho, G. Wu, Transition metal (Fe, Co, Ni, and Mn) oxides for oxygen reduction and evolution bifunctional catalysts in alkaline media, Nano Today 11 (2016).
[54] Y. Gorlin, B. Lassalle-Kaiser, J.D. Benck, S. Gul, S.M. Webb, V.K. Yachandra, J. Yano, T.F. Jaramillo, In situ X-ray absorption spectroscopy investigation of a bifunctional manganese oxide catalyst with high activity for electrochemical water oxidation and oxygen reduction, J. Am. Chem. Soc. 135 (2013) 8525–8534.
[55] T.Y. Ma, S. Dai, M. Jaroniec, S.Z. Qiao, Metal–Organic Framework Derived Hybrid Co3O4-Carbon Porous Nanowire Arrays as Reversible Oxygen Evolution Electrodes, J. Am. Chem. Soc. 136 (2014) 13925–13931.
[56] R. Gao, J. Zhu, X. Xiao, Z. Hu, J. Liu, X. Liu, Facet-Dependent Electrocatalytic Performance of Co3O4 for Rechargeable Li–O2 Battery, J. Phys. Chem. C 119 (2015) 4516–4523.
[57] C. Li, X. Han, F. Cheng, Y. Hu, C. Chen, J. Chen, Phase and composition controllable synthesis of cobalt manganese spinel nanoparticles towards efficient oxygen electrocatalysis, Nat. Commun. 6 (2015) 7345.
[58] S. Peng, Y. Hu, L. Li, X. Han, F. Cheng, M. Srinivasan, Q. Yan, S. Ramakrishna, J. Chen, Controlled synthesis of porous spinel cobaltite core-shell microspheres as high-performance catalysts for rechargeable Li–O2 batteries, Nano Energy 13 (2015) 718–726.
[59] T. Maiyalagan, K.A. Jarvis, S. Therese, P.J. Ferreira, A. Manthiram, Spinel-type lithium cobalt oxide as a bifunctional electrocatalyst for the oxygen evolution and oxygen reduction reactions, Nat. Commun. 5 (2014) 3949.

[60] I. Yamada, H. Fujii, A. Takamatsu, H. Ikeno, K. Wada, H. Tsukasaki, S. Kawaguchi, S. Mori, S. Yagi, Bifunctional Oxygen Reaction Catalysis of Quadruple Manganese Perovskites, Adv. Mater. 29 (2017) 1603004.
[61] E.F. Sheka, N.N. Rozhkova, Shungite as the natural pantry of nanoscale reduced graphene oxide, International Journal of Smart and Nano Materials. 5 (2014) 1–16.
[62] K. N. Wood, R. O'Hayre, S. Pylypenko, Recent progress on nitrogen/carbon structures designed for use in energy and sustainability applications, Energy Environ. Sci. 7 (2014) 1212–1249.
[63] B.Y. Xia, Y. Yan, N. Li, H.B. Wu, X.W. (David) Lou, X. Wang, A metal–organic framework-derived bifunctional oxygen electrocatalyst, Nat. Energy 1 (2016) 1–8.
[64] J.-C. Li, P.-X. Hou, S.-Y. Zhao, C. Liu, D.-M. Tang, M. Cheng, F. Zhang, H.-M. Cheng, A 3D bi-functional porous N-doped carbon microtube sponge electrocatalyst for oxygen reduction and oxygen evolution reactions, Energy Environ. Sci. 9 (2016) 3079–3084.
[65] Molecule-Level g-C3N4 Coordinated Transition Metals as a New Class of Electrocatalysts for Oxygen Electrode Reactions. - PubMed - NCBI, (2020).
[66] F. Meng, H. Zhong, D. Bao, J. Yan, X. Zhang, In Situ Coupling of Strung Co4N and Intertwined N-C Fibers toward Free-Standing Bifunctional Cathode for Robust, Efficient, and Flexible Zn-Air Batteries, J. Am. Chem. Soc. 138 (2016) 10226–10231.
[67] N.H. Chou, N. Pierce, Y. Lei, N. Perea-López, K. Fujisawa, S. Subramanian, J.A. Robinson, G. Chen, K. Omichi, S.S. Rozhkov, N.N. Rozhkova, M. Terrones, A.R. Harutyunyan, Carbon-rich shungite as a natural resource for efficient Li-ion battery electrodes, Carbon 130 (2018) 105–111.
[68] S.K. Tiwari, V. Kumar, A. Huczko, R. Oraon, A.D. Adhikari, G.C. Nayak, Magical Allotropes of Carbon: Prospects and Applications, Crit. Rev. Solid State Mater. Sci. 41 (2016) 257–317.
[69] R. Gusmão, Z. Sofer, D. Bouša, M. Pumera, Synergetic Metals on Carbocatalyst Shungite, Chem. Eur. J. 23 (2017) 18232–18238.
[70] P. Buseck, D. GeologyandChenistryA, L.P. Galdobina, Shungites: The C-rich rocks of Carelia, Russia, The Canadian Mineralogist 35 (1997) 1363-1378.
[71] E. Tamburri, R. Carcione, S. Politi, M. Angjellari, L. Lazzarini, L.E. Vanzetti, S. Macis, G. Pepponi, M.L. Terranova, Shungite Carbon as Unexpected Natural Source of Few-Layer Graphene Platelets in a Low Oxidation State, Inorg. Chem. 57 (2018) 8487–8498.
[72] K.D. Sattler, Carbon Nanomaterials Sourcebook: Graphene, Fullerenes, Nanotubes, and Nanodiamonds, Volume I, CRC Press, 2016.
[73] S.Y. Chazhengina, V.V. Kovalevski, Structural characteristics of shungite carbon subjected to contact metamorphism overprinted by greenschist-facies regional metamorphism, Eur. J. Mineral. 25 (2013) 835–843.
[74] V.A. Melezhik, M.M. Filippov, A.E. Romashkin, A giant Palaeoproterozoic deposit of shungite in NW Russia: genesis and practical applications, Ore Geol. Rev. 24 (2004) 135–154.
[75] S.V. Krasnovyd, A.A. Konchits, B.D. Shanina, M.Y. Valakh, I.B. Yanchuk, V.O. Yukhymchuk, A.V. Yefanov, M.A. Skoryk, Local structure and paramagnetic properties of the nanostructured carbonaceous material shungite, Nanoscale Res Lett. 10 (2015) 78.
[76] P. Hu, Y. Song, L. Chen, S. Chen, Electrocatalytic activity of alkyne-functionalized AgAu alloy nanoparticles for oxygen reduction in alkaline media, Nanoscale. 7 (2015) 9627–9636.
[77] A.J. Bard, L.R. Faulkner, Electrochemical methods: fundamentals and applications, 2nd ed, Wiley, New York, 2001.

[78] R.R. Adžić, J. Wang, B.M. Ocko, Structure of metal adlayers during the course of electrocatalytic reactions: O2 reduction on Au(111) with Tl adlayers in acid solutions, Electrochim. Acta 40 (1995) 83–89.
[79] D.R. Lide, CRC handbook of chemistry and physics, CRC Press, Boca Raton, 2000.
[80] A. Das, S. Pisana, B. Chakraborty, S. Piscanec, S.K. Saha, U.V. Waghmare, K.S. Novoselov, H.R. Krishnamurthy, A.K. Geim, A.C. Ferrari, A.K. Sood, Monitoring dopants by Raman scattering in an electrochemically top-gated graphene transistor, Nat. Nanotechnol. 3 (2008) 210–215.
[81] X. Xiao, X. Li, G. Yu, J. Wang, G. Yan, Z. Wang, H. Guo, FeCox alloy nanoparticles encapsulated in three-dimensionally N-doped porous carbon/multiwalled carbon nanotubes composites as bifunctional electrocatalyst for zinc-air battery, J. Power Sources 438 (2019) 227019.
[82] Y.-J. Wang, H. Fan, A. Ignaszak, L. Zhang, S. Shao, D.P. Wilkinson, J. Zhang, Compositing doped-carbon with metals, non-metals, metal oxides, metal nitrides and other materials to form bifunctional electrocatalysts to enhance metal-air battery oxygen reduction and evolution reactions, Chem. Eng. J. 348 (2018) 416–437.
[83] J. Sun, Y. Yang, J. Wang, Z. Zhang, J. Guo, In-situ construction of cobalt oxide/ nitrogen-doped porous carbon compounds as efficient bifunctional catalysts for oxygen electrode reactions, J. Alloys Comp. 827 (2020) 154308.
[84] D. Chen, J. Zhu, X. Mu, R. Cheng, W. Li, S. Liu, Z. Pu, C. Lin, S. Mu, Nitrogen-Doped carbon coupled FeNi3 intermetallic compound as advanced bifunctional electrocatalyst for OER, ORR and zn-air batteries, Appl. Catal. B: Environ. 268 (2020) 118729.
[85] M. Lefèvre, E. Proietti, F. Jaouen, J.-P. Dodelet, Iron-based catalysts with improved oxygen reduction activity in polymer electrolyte fuel cells, Science 324 (2009) 71–74.
[86] T.-H. You, C.-C. Hu, Designing Binary Ru–Sn Oxides with Optimized Performances for the Air Electrode of Rechargeable Zinc–Air Batteries, ACS Appl. Mater. Interfaces 10 (2018) 10064–10075.
[87] Y.J. Sa, K. Kwon, J.Y. Cheon, F. Kleitz, S.H. Joo, Ordered mesoporous Co3O4 spinels as stable, bifunctional, noble metal-free oxygen electrocatalysts, J. Mater. Chem. A 1 (2013) 9992–10001.
[88] L. Gui, Z. Huang, D. Ai, B. He, W. Zhou, J. Sun, J. Xu, Q. Wang, L. Zhao, Integrated Ultrafine Co0.85Se in Carbon Nanofibers: An Efficient and Robust Bifunctional Catalyst for Oxygen Electrocatalysis, Chem. Eur. J. 26 (2020) 4063–4069.

SUPPLEMENTARY INFORMATION

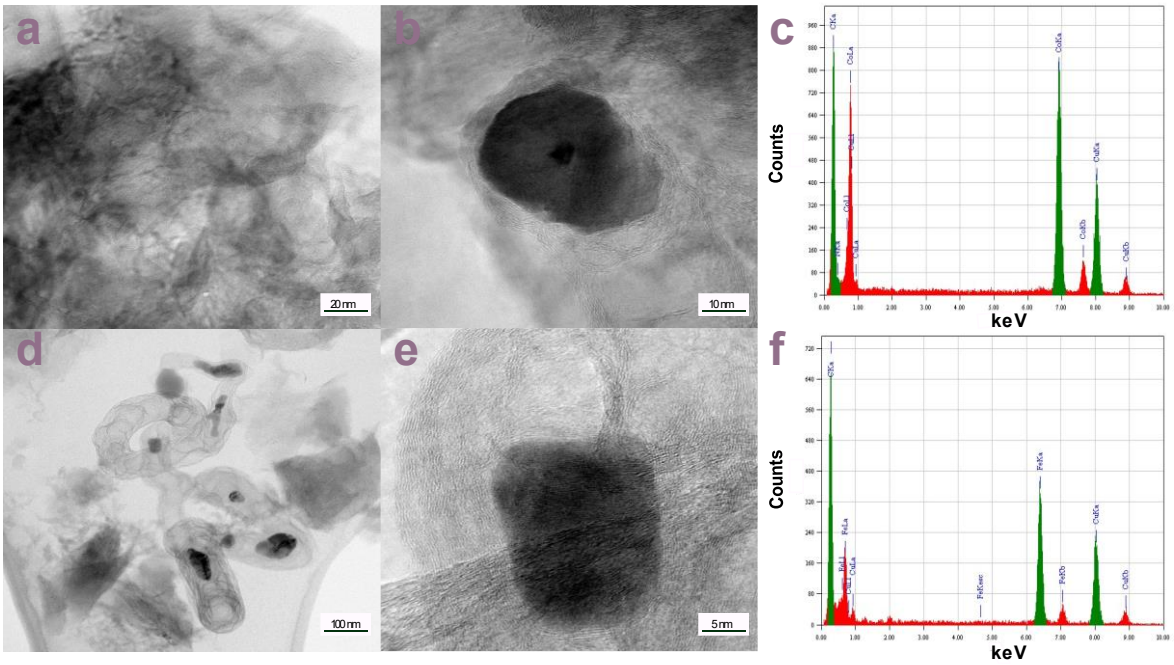

Figure S1. TEM/HRTEM images and EDS spectra of (a-c) SH3DCDA-Co and (d-f) SH3DCDA-Fe samples.

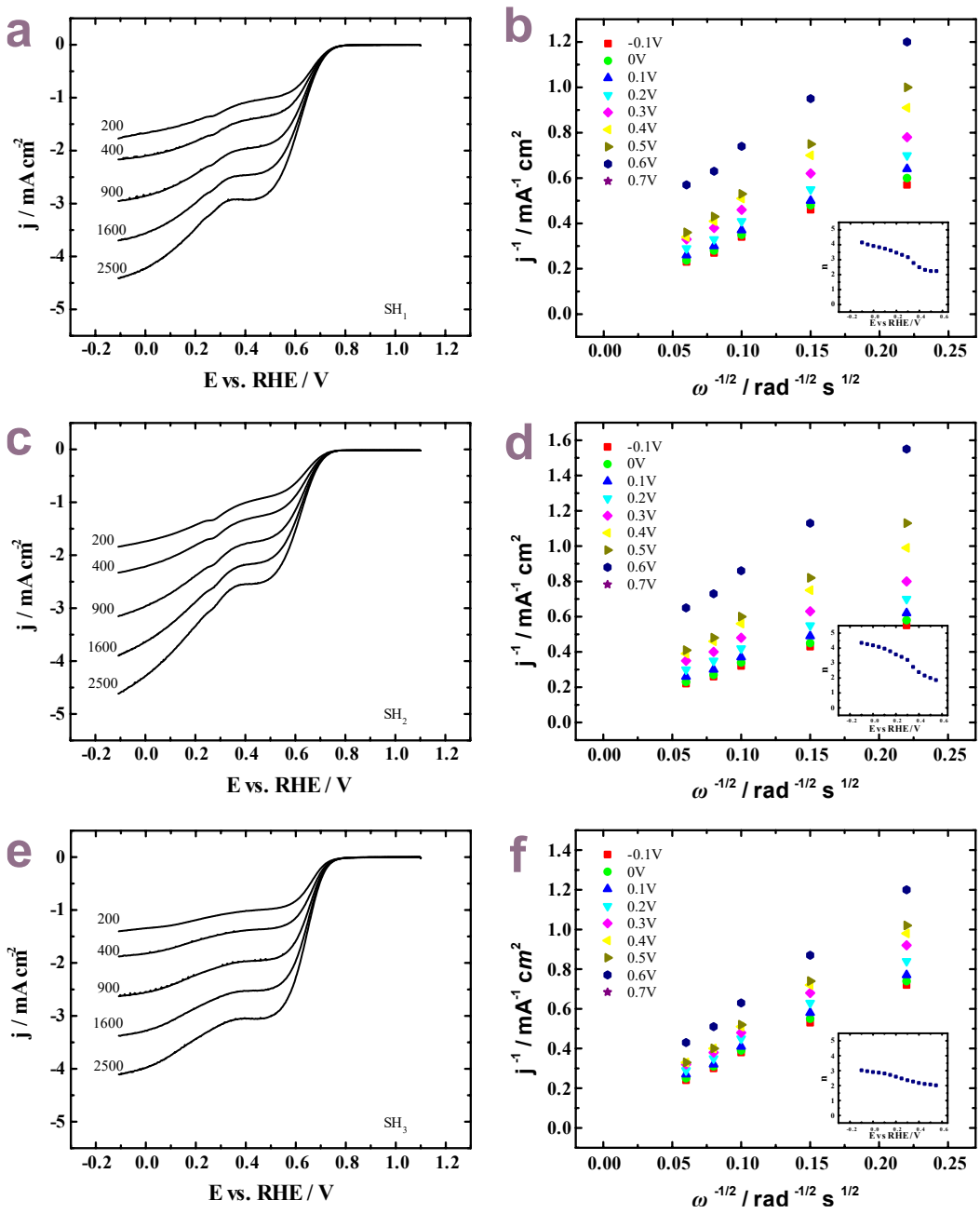
a
b
c
d
e
f
j / mA cm-2
E vs. RHE / V
200
400
900
1600
2500
SH1
SH2
SH3
j-1 / mA-1 cm2
ω -1/2 / rad -1/2 s 1/2
-0.1V
0V
0.1V
0.2V
0.3V
0.4V
0.5V
0.6V
0.7V
n
E vs RHE / V

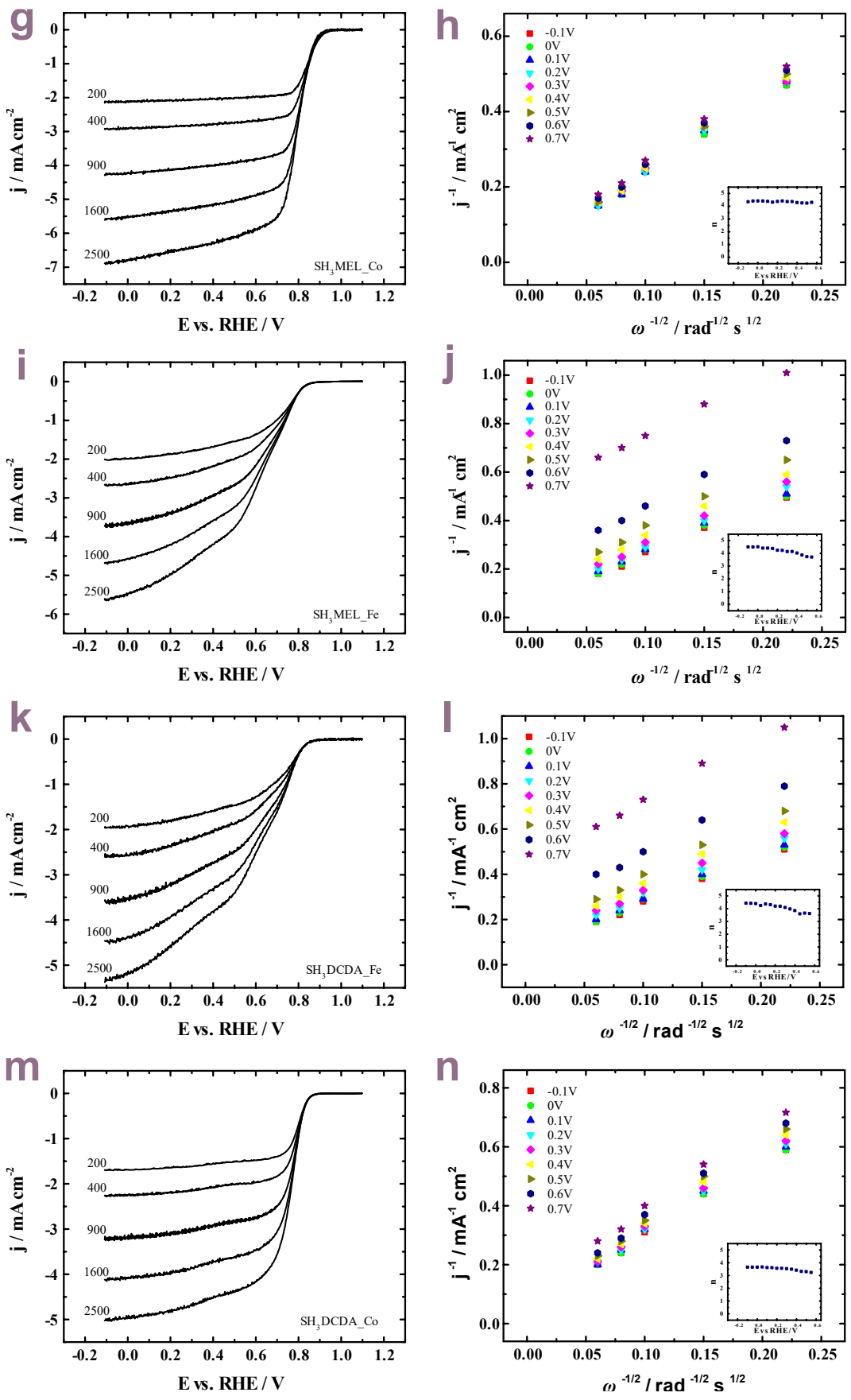

Figure S2. ORR polarization curves and K-L plots; insets: *n* as a function of potential.

Table S1. Some state-of-the-art bifunctional ORR/OER catalyst in 0.1 M KOH.

Catalyst	Loading, electrolyte	$E_{1/2}$ / V	E_{10} / V	ΔE / V	Ref.
Fe-N-C	0.4 mg cm^{-2} 0.1 M KOH	0.84	1.60	0.76	[85]
$RuSn_{73}$	0.1 mg cm^{-2} 0.1 M KOH	0.52	1.49	0.97	[86]
Co-N-C	0.2 mg cm^{-2} 0.1 M KOH	0.80	1.54	0.74	[66]
meso-Co_3O_4-100	0.1mg_{cat} cm^{-2} 0.1 M KOH	0.61	1.66	1.05	[87]
S,N-Fe/N/C-CNT	- 0.1 M KOH	0.85	-	0.75	[48]
Co_3O_4/NPC	0.77 mg cm^{-2} 0.1 M KOH	0.82	-	0.8	[83]
$FeNi_3$@NC	2.0 mg·cm^{-2} 0.1 M KOH	0.86	-	0.65	[84]
$Co_{0.85}$Se@CNFs	0.2264 mg_{cat} cm^{-2} 0.1 M KOH	0.82	-	0.74	[88]

NON-EXCLUSIVE LICENCE TO REPRODUCE THESIS AND MAKE THESIS PUBLIC

I, Nargiz Kazimova

1. herewith grant the University of Tartu a free permit (non-exclusive licence) to reproduce, for the purpose of preservation, including for adding to the DSpace digital archives until the expiry of the term of copyright,

"Shungite as a catalyst support for highly active bifunctional oxygen electrocatalyst"

supervised by Nadezda Kongi.

2. I grant the University of Tartu a permit to make the work specified in p. 1 available to the public via the web environment of the University of Tartu, including via the DSpace digital archives, under the Creative Commons licence CC BY NC ND 3.0, which allows, by giving appropriate credit to the author, to reproduce, distribute the work and communicate it to the public, and prohibits the creation of derivative works and any commercial use of the work until the expiry of the term of copyright.

3. I am aware of the fact that the author retains the rights specified in p. 1 and 2.

4. I certify that granting the non-exclusive licence does not infringe other persons' intellectual property rights or rights arising from the personal data protection legislation.

Nargiz Kazimova

20/05/2020